2 Steady-State Performance and Analytic Derivation of SRM Characteristics

2.1 INTRODUCTION

The requirement for finding the performance characteristics of the SRM is to generate the relationships between the flux linkages vs. rotor position as a function of the machine phase currents. This section develops a procedure for analytically deriving the machine characteristics given the motor dimensions and excitation conditions along with the number of turns per phase. Notably, the nonlinear characteristics of the lamination material are preserved in this method to get a meaningful characterization of the SRM.

2.2 DATA FOR PERFORMANCE COMPUTATION

The area enclosed between the curves λ vs. i for unaligned and aligned positions of the rotor poles with a set of stator poles gives the maximum work done for one stroke of the motor. The electromagnetic torque can then be calculated if the angular movement is known from the mechanical work. Even though the calculation of torque and work done appears to be simple, the data generation for their calculation is a complex process. The data required for this procedure are the flux linkages vs. stator excitation currents for discrete positions of the rotor.

The aligned position corresponds to the center of the stator and rotor poles coinciding, and the unaligned position with the midpoint of the interpolar rotor gap facing the stator pole. It is possible to calculate the flux linkages for the aligned position analytically due to the fact that the leakage flux is negligible in the aligned position. The same is not true for the unaligned position; because the leakage paths are not known *a priori*, it is not easy to calculate the leakage flux analytically. Finite element analysis techniques are used to estimate the flux linkages.

Figures 2.1 and 2.2 show the flux at the unaligned position in a 6/4-pole[6,7,8] and 12/10-pole SRM,[2] respectively. It is clear from these figures that the flux paths in the unaligned positions are very difficult to predict, thus the complexity of the steady-state performance evaluation. It is usual to use finite element analysis techniques to map the flux in the unaligned position and for positions in between the aligned and unaligned stator and rotor poles. The flux leakage in the aligned position is practically

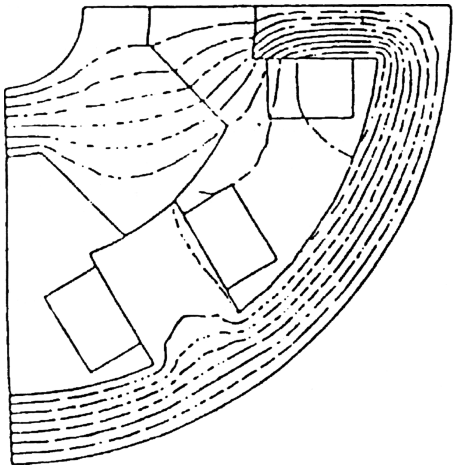

FIGURE 2.1 Flux plot at fully unaligned position for 6/4 SRM.

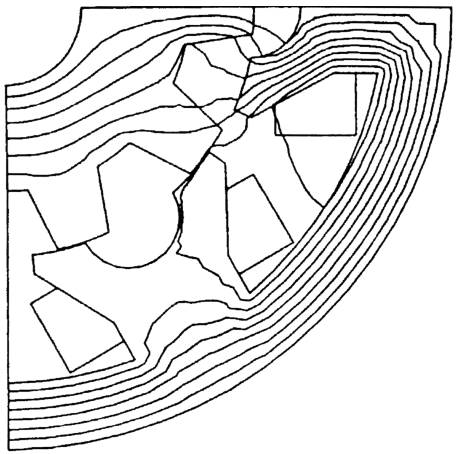

FIGURE 2.2 Flux plot at fully unaligned position for 12/10 SRM.

negligible (as shown in Figures 2.3 and 2.4) for the 6/4 and 12/10 SRMs, respectively; therefore, the analytical calculation of the stator flux linkages at the aligned position is very accurate. The accuracy usually is within 2% of the finite element solution.

2.3 ANALYTIC METHOD FOR THE COMPUTATION OF MOTOR FLUX LINKAGES

The performance of the switched reluctance motor can be computed by finite element analysis techniques, but there are some disadvantages in resorting to them routinely. The relationship of motor output variables to motor dimensions, number of poles, number of turns per phase, excitation current, and current conduction angle

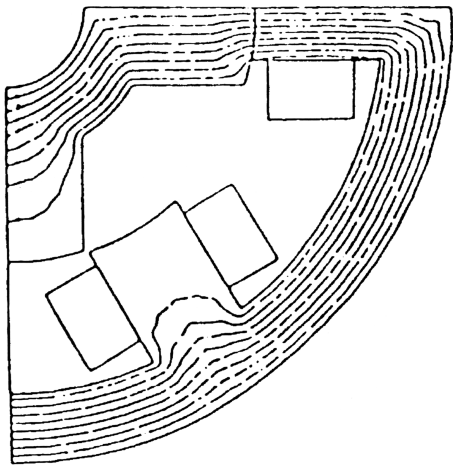

FIGURE 2.3 Flux plot at fully aligned position for 6/4 SRM.

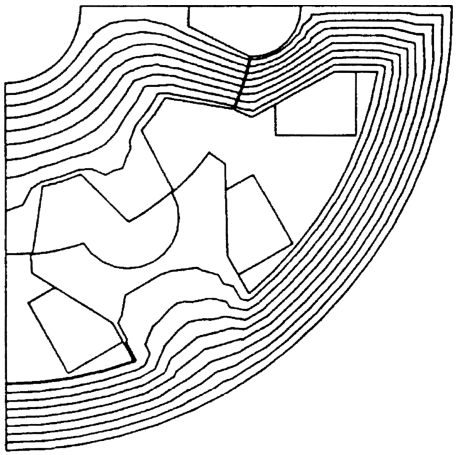

FIGURE 2.4 Flux plot at fully aligned position for 12/10 SRM.

is not explicit. Hence, a change in one or many of the motor and control variables requires an entire finite element analysis computation which is either in two or three dimensions. Each set of finite element computations takes a considerable amount of time. Needless to say, such results are not valid for up and down scaling of the motor design. The scaling of the motors is very essential in a design environment, as the design of the motor is continually assessed to optimize a performance index. The performance index can be cost, efficiency, weight, volume, torque, output, or a combination of these for the switched reluctance motor and converter combination. In such a case, a design process to obtain a size and to evaluate variables of interest for the machine will be mandatory. The process has to be based on a set of implicit and

explicit analytical expressions involving the motor dimensions and inputs to performance variables.[1,3,4,5,10,11,12,14,15] The final design emerging from this analytic design approach can be analyzed with finite element modeling to improve the accuracy of the performance prediction. The following section gives an analytic approach that uses numerical iteration to obtain inductance vs. current characteristics of the motor from machine variables that are used to predict the torque and power output.

The procedure outlined in this chapter is to find inductance vs. rotor position vs. excitation current; that data is necessary to design the converter and controllers. The inductances are easier to deal with in the context of power electronics networks than flux linkages, but the flux linkages are very crucial to find the air gap torque and hence performance of the machine. Obtaining flux linkages from inductance and the excitation current by taking their product is fairly straightforward. From now on, the evaluation of flux linkages will not be mentioned in this chapter; only inductance evaluation is emphasized.

2.3.1 Method of Inductance Calculation

For various positions of the rotor, a fixed number of flux paths is assumed. In order to minimize the number of flux maps for evaluation of inductance, only four flux maps are considered: the extreme positions of unalignment and alignment of rotor and stator poles and, in between these two extremes, two regions defined for overlapping and nonoverlapping rotor and stator poles. A generalization for various numbers of stator and rotor poles can be made in the derivation of relevant equations required in the inductance calculation (not considered in detail here).

Flux maps are usually derived based on the experience of the designer and can be fine tuned with the finite element analysis tool to improve the accuracy of the flux paths. A two-dimensional field analysis using finite element software is sufficient for most applications. Critical applications with a high power-density requirement for SRMs can be met with a three-dimensional field analysis. To a degree, the three-dimensional effects can also be included in the analytic procedure and will be indicated at appropriate instances in the derivations.

An SRM with an 8/6-pole combination is considered for deriving the analytic procedure for inductance evaluation. Assume a certain flux density in the stator pole and flux densities in other parts of the machine such as rotor pole, rotor back iron, stator yoke, and air gap are derived as the areas of cross sections of these parts for assumed flux paths are obtained from the machine geometry and the assumed stator pole flux density. From the flux densities in various parts of the machine and the flux density vs. magnetic field intensity (B-H) characteristics of the lamination material, corresponding magnetic field intensities are obtained. Given the magnetic field intensities and the length of the flux path in each part, their product gives the magnetomotive force (mmf). The mmfs for various parts are likewise obtained, and for the magnetic equivalent circuit and stator excitation Ampere's circuital law is applied. If an error between the applied stator mmf and that given equivalently by various parts of the machine reveals a discrepancy, then that error is used to adjust the assumed flux density in the stator pole and the entire iteration continues until the error is reduced to a set tolerance value.

2.3.1.1 Flux Density Evaluation

For example, consider the complete unaligned position and flux path 1 shown in Figure 2.5 to illustrate the procedure for evaluating flux densities in various parts of the machine. The flux paths are equiflux lines (i.e., equal amount of flux lines are represented by each flux path). The flux distribution is symmetric with respect to the center line of the excited stator poles. The flux path 1 is assumed to have a flux of ϕ_1 in the stator pole. It crosses the air gap, splits evenly in the rotor back iron, and then recrosses the air gap to the southern pole and splits evenly to flow in the stator back iron (yoke). The reluctances of the stator pole, air gap, rotor back iron, and stator back iron for the flux path are denoted as R_{sp1}, R_{g1}, R_{ry1}, and R_{sy1}, respectively. The magnetic equivalent circuit for flux path 1 in terms of the reluctances and stator mmf, F_1, is shown in Figure 2.6. The equivalent circuit is then simplified and given in Figure 2.7. From Figure 2.6, the flux in each segment of the machine is known and accordingly the flux densities for these segments are evaluated. Let the area of cross section of flux path 1 in the stator pole, air gap, rotor back iron, and stator back iron be A_{sp1}, A_{g1}, A_{ry1}, and A_{sy1}, respectively. If the stator flux density is B_{sp}, then the flux in path 1 in the stator is found if the area of cross section for the flux path is known. The flux path encloses one quarter of the stator pole arc; therefore, the area of cross section is

$$A_{sp1} = \frac{1}{4}(\text{stator pole area}) = \frac{1}{4}\left(\frac{D}{2}\beta_s \cdot L\right) = \frac{1}{8}(DL)\beta_s \tag{2.1}$$

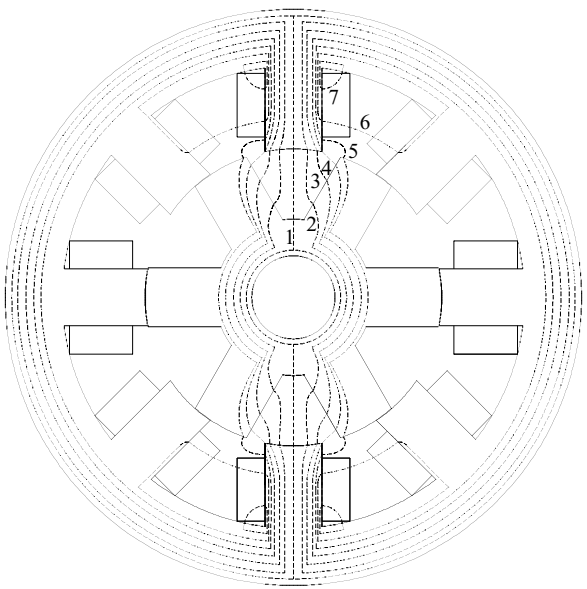

FIGURE 2.5 Identification of seven flux paths for analytical calculation of unaligned inductance.

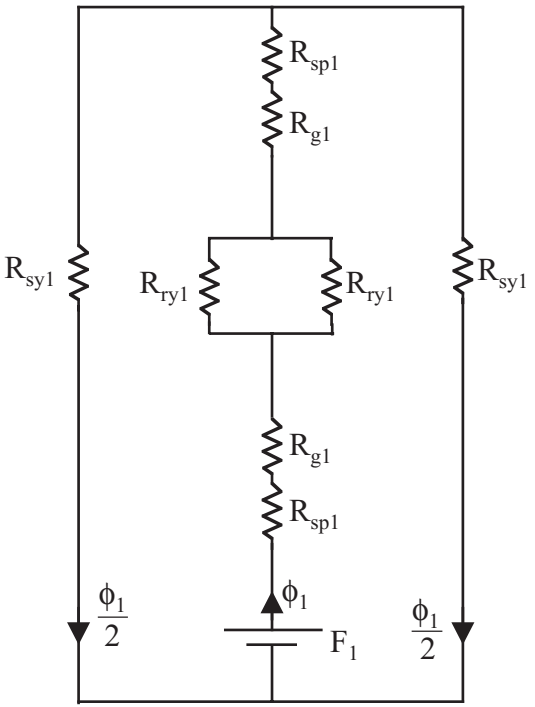

FIGURE 2.6 Magnetic equivalent circuit for flux path 1 at fully unaligned position.

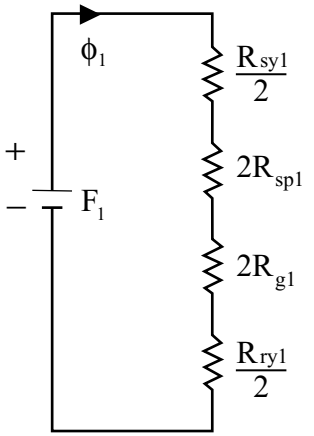

FIGURE 2.7 Simplified magnetic equivalent circuit for flux path 1 at fully unaligned position.

where D is the inner stator lamination diameter, β_s is the stator pole arc, and L is the stator iron stack length.

Then the stator pole flux in path 1 is

$$\phi_1 = B_{sp} \cdot A_{sp1} \tag{2.2}$$

Let the mean area of the cross section of the air gap, rotor back iron, and stator back iron be, A_{g1}, A_{ry1}, and A_{sy1}, respectively. Then the flux densities in these segments are

$$B_{g1} = \frac{\phi_1}{A_{g1}} = B_{sp} \cdot \left(\frac{A_{sp1}}{A_{g1}}\right) \tag{2.3}$$

$$B_{ry1} = \frac{\phi_1}{2A_{ry1}} = \frac{B_{sp}}{2} \cdot \left(\frac{A_{sp1}}{A_{ry1}}\right) \tag{2.4}$$

$$B_{sy1} = \frac{\phi_1}{2A_{sy1}} = \frac{B_{sp}}{2} \cdot \left(\frac{A_{sp1}}{A_{sy1}}\right) \tag{2.5}$$

$$B_{sp1} = B_{sp} \tag{2.6}$$

2.3.1.2 mmf Evaluation

The mmf for each segment of the flux path is evaluated by finding the magnetic field intensities from the flux densities of the segments using the B-H characteristics of the lamination material and average length of the flux path in the segments. Let the magnetic field intensities of the stator pole, air gap, rotor back iron, and stator back iron segments be H_{sp1}, H_{g1}, H_{ry1}, and H_{sy1}, respectively. The average lengths of the flux path 1 in the stator pole, air gap, rotor back iron, and stator back iron are ℓ_{sp1}, ℓ_{g1}, ℓ_{ry1}, and ℓ_{sy1}, respectively. Then, the Ampere circuital equation for this path is

$$F_1 = T_{ph} i = \Sigma H \ell = 2[H_{sp1}\ell_{sp1} + H_g \ell_{g1}] + \frac{1}{2}[H_{ry1}\ell_{ry1} + H_{sy1}\ell_{sy1}] \tag{2.7}$$

If the computed right-hand side is not equal to the applied mmf, F_1, then the error between them is a mark of incorrect flux densities in various segments of the machine. The error between the applied and computed mmf can be reduced to a level that is acceptable by an iterative adjustment of the stator pole flux density, B_{sp}, and then recalculating all the other variables. Let the error mmf be defined as:

$$\Delta F_1 = F_1 - \Sigma H \ell = T_{ph} i - \Sigma H \ell \tag{2.8}$$

If the error mmf is negative, then the stator pole flux density is reduced for the next iteration; in the case of a positive error, the stator pole flux density is increased for the next iteration. Nulling the mmf error is not attempted in practice due to the large number of iterations; therefore, the mmf error is reduced to a lower tolerance limit.

2.3.1.3 Calculation of Reluctance

From the final flux densities in the various segments of flux path 1 and the magnetic field intensities, the reluctances are computed. The reluctance of the stator pole segment is

$$R_{sp1} = \frac{\ell_{sp1}}{A_{sp1}\mu_o\mu_r} = \frac{\ell_{sp1}}{A_{sp1}\cdot\left(\frac{B_{sp1}}{H_{sp1}}\right)} = \frac{H_{sp1}\ell_{sp1}}{B_{sp1}A_{sp1}} \tag{2.9}$$

Similarly, the reluctances of the air gap, rotor back iron, and stator back iron are

$$R_{g1} = \frac{\ell_{g1}}{\mu_o A_{g1}} \tag{2.10}$$

$$R_{ry1} = \frac{H_{ry1}\ell_{ry1}}{B_{ry1}A_{ry1}} \tag{2.11}$$

$$R_{sy1} = \frac{H_{sy1}\ell_{sy1}}{B_{sy1}A_{sy1}} \tag{2.12}$$

In all these computations for all the flux paths, the mean length and their area of cross section are required, which we derive in the following.

2.3.1.4 Assumptions

The equations derived in this chapter apply to all levels of excitation under the assumptions stated below:

1. The air gap flux lines consist of concentric arcs and straight-line segments.
2. The flux lines enter and leave the iron normally.
3. The flux lines in the stator and rotor poles are parallel to the pole axes.
4. The flux lines in the stator back iron and rotor body are concentric.
5. The windings are rectangular blocks and the stator interpolar space is only partially filled with windings.
6. The shaft is purely nonmagnetic.

These assumptions make analytic derivations easier and approximate real conditions in the machine.

2.3.2 Unaligned Inductance

Aligned inductance for a given excitation current is derived in this section using the procedure outlined in the previous section. The flux paths at a completely unaligned position are shown in Figure 2.5. Each of the flux paths is considered separately and inductance contributed by it is derived. The computational procedure to evaluate the path inductance is developed, along with a flow chart for mechanization. Various angles defined are only relevant to the flux path under consideration, so care needs to be exercised when defining them for various flux paths for programming.

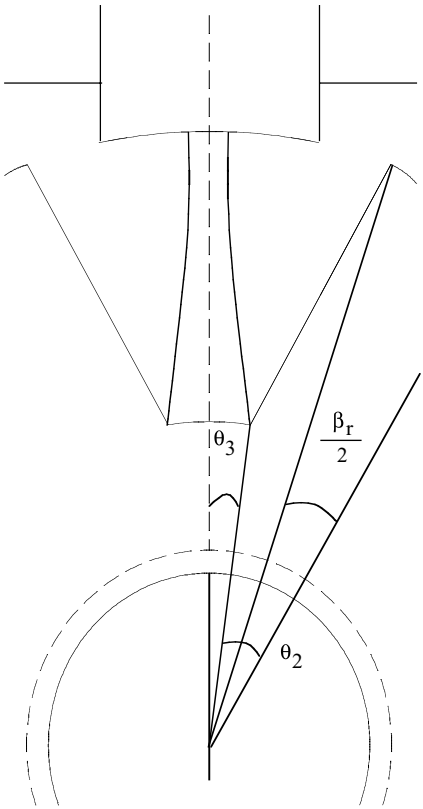

FIGURE 2.8 Flux path 1 in fully unaligned position.

2.3.2.1 Flux Path 1

The calculation of the mean flux path in the air gap between the stator and rotor poles is considered first. That segment is expanded and shown in Figure 2.8. The area of cross section at the stator pole for the path has been derived in Eq. (2.1). The length of the flux path in the air gap is

$$\ell_{g1} = \frac{D}{2} - \ell_g - h_r \tag{2.13}$$

where ℓ_g is the air gap during alignment, and h_r is the rotor pole height.

The area of cross section of flux path 1 is varying throughout the air gap so its mean is considered for calculation. The cross section of the flux path at the rotor is obtained as follows:

$$\theta_2 = \frac{\dfrac{\beta_r\left(\dfrac{D}{2} - \ell_g\right)}{2}}{\left(\dfrac{D}{2} - \ell_g - h_r\right)} \tag{2.14}$$

It is assumed that the rotor pole width remains constant over its length, which usually is the case. Then, θ_3 is derived as:

$$\theta_3 = \frac{1}{2}\left(\frac{2\pi}{P_r}\right) - \theta_2 = \frac{\theta_{rp}}{2} - \theta_2 \tag{2.15}$$

where θ_{rp} is the rotor pole pitch, and P_r is the number of rotor poles. The area of cross section on the rotor periphery is

$$A_{r1} = 2\theta_3\left(\frac{D}{2} - \ell_g - h_r\right)L \tag{2.16}$$

and the average area of cross section of flux path 1 is

$$A_{g1} = \frac{A_{sp1} + A_{r1}}{2} = \frac{\beta_s DL}{16} + \theta_3\left(\frac{D}{2} - \ell_g - h_r\right)L \tag{2.17}$$

2.3.2.1.1 Rotor Back Iron

The length of the flux path on each side of the rotor back iron is

$$\ell_{ry1} = \frac{1}{2}[\text{average of } \{\text{periphery of shaft + periphery of inner rotor pole base}\}]$$

$$= \frac{1}{2}\left[\frac{\pi D_{sh}}{2} + \pi\left(\frac{D}{2} - \ell_g - h_r\right)\right] = \pi\left(\frac{D_{sh}}{4} + \frac{D}{4} - \frac{\ell_g}{2} - \frac{h_r}{2}\right) \tag{2.18}$$

where D_{sh} is the rotor shaft diameter. The area of cross section of the rotor back iron for this flux path is

$$A_{ry1} = \left(\frac{D}{2} - \ell_g - h_r - \frac{D_{sh}}{2}\right)L \tag{2.19}$$

where the quantity inside the parentheses is the thickness of the rotor back iron.

2.3.2.1.2 Stator Pole

The length of the flux path in the stator is

$$\ell_{sp1} = h_s \tag{2.20}$$

where h_s is the stator pole height. Its cross section has been already derived.

2.3.2.1.3 Stator Back Iron

The length of the flux path in the stator back iron is

$$\ell_{sy1} = \frac{\pi(D_o - b_{sy})}{2} = \frac{\pi(D + 2h_s + 2b_{sy} - b_{sy})}{2} = \frac{\pi(D + 2h_s + b_{sy})}{2} \tag{2.21}$$

where b_{sy} is the stator back iron thickness. Its area of cross section is

$$A_{sy1} = b_{sy}L \tag{2.22}$$

This completes the relevant variables and constants for the computation of reluctances for flux path 1. The inductance contributed by the flux path 1 at unaligned inductance, then, is

$$L_{u1} = \frac{T_{ph} \cdot \phi_1}{i} = \frac{T_{ph} \cdot \dfrac{F_1}{\left(2R_{sp1} + 2R_{g1} + \dfrac{R_{sy1}}{2} + \dfrac{R_{ry1}}{2}\right)}}{i} = \frac{T_{ph}^2}{\left(2R_{sp1} + 2R_{g1} + \dfrac{R_{sy1}}{2} + \dfrac{R_{ry1}}{2}\right)} \tag{2.23}$$

The flux ϕ_1 is computed from the magnetic equivalent circuit in the final iteration to satisfy Ampere's circuital law, as discussed earlier in this section. A flow chart of the procedure involved in the computation of inductance is shown in Figure 2.9. For relevant equations in each block of the flow chart, refer to the derivations in this section.

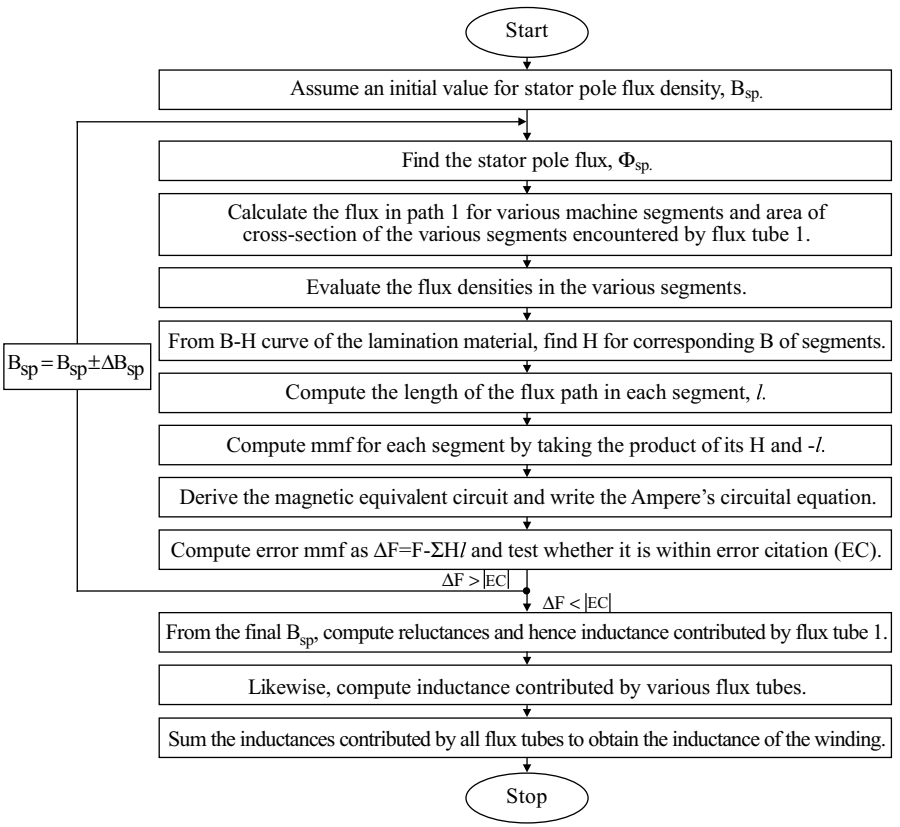

FIGURE 2.9 Flow chart for the evaluation of machine inductance.

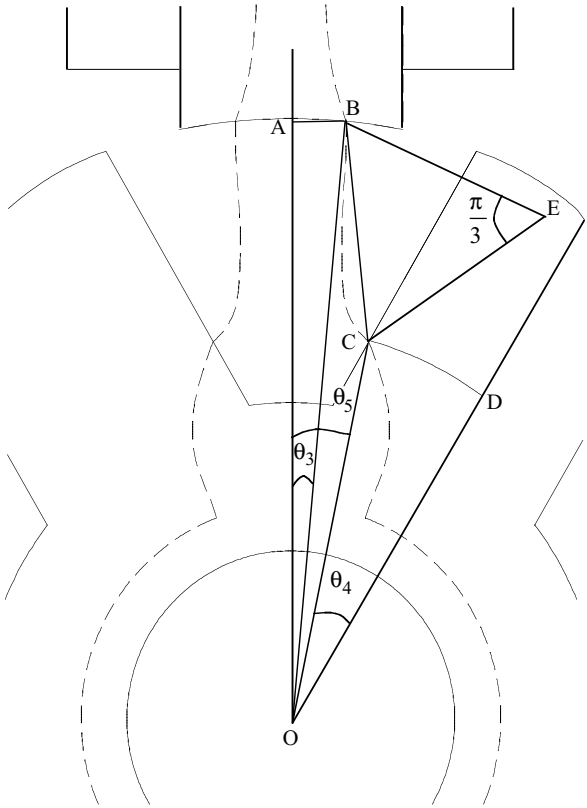

FIGURE 2.10 Flux path 2 in fully unaligned position.

2.3.2.2 Flux Path 2

An enlarged upper part of flux path 2 is shown in Figure 2.10, and the magnetic equivalent circuit is shown in Figure 2.11, where F_2 is the mmf applied on the stator pole. Only one side is considered for the equivalent circuit. For flux path 2, R_{sp2} is the stator pole reluctance, R_{g2} is the air gap reluctance, R_{rp2} is the rotor back iron reluctance, and R_{sy2} is the reluctance of the stator back iron. For these segments, the area of cross section and length of the flux path are derived in the following. It is assumed that the flux enters at $(h_r/4)$ from the inner radius at the rotor pole.

2.3.2.2.1 Air Gap

Consider the length of flux path 2 to be the arc *BC*. It is computed by finding the chord length *BC* and using this as a radius by constructing an equilateral triangle, *BCE*. Assume that the center of the shaft is origin (0, 0). The steps are as follows:

$$OB = \frac{D}{2} \tag{2.24}$$

$$\theta_3 = \frac{\beta_s}{4} \tag{2.25}$$

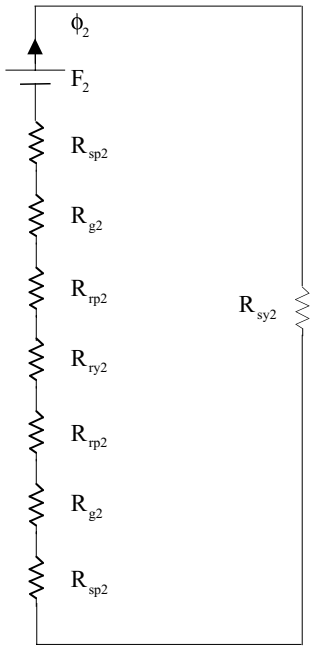

FIGURE 2.11 Magnetic equivalent circuit for flux path 2 for one side of the machine.

The coordinates of B with O as origin are

$$(x_1, y_1) = \left[\frac{D}{2}\sin(\theta_3), \frac{D}{2}\cos(\theta_3)\right] \tag{2.26}$$

The coordinates of $C(x_2, y_2)$ are found as:

$$OD = \left(\frac{D}{2} - \ell_g - \frac{3}{4}h_r\right) \tag{2.27}$$

$$CD = \left(\frac{D}{2} - \ell_g\right)\frac{\beta_r}{2} \tag{2.28}$$

$$\theta_4 = \frac{CD}{OD} \tag{2.29}$$

$$\underline{|COA} = \theta_5 = \frac{\theta_{rp}}{2} - \theta_4 \tag{2.30}$$

$$(x_2, y_2) = [OD\sin(\theta_5), OD\cos(\theta_5)] \tag{2.31}$$

The chord BC is, then:

$$BC = \sqrt{(x_2 - x_1)^2 + (y_2 - y_1)^2} \tag{2.32}$$

Then, the length of the flux in path 2 may be considered as arc BC. The arc is evaluated by considering an equilateral triangle BCE with the length of each side BC, and the arc is part of the circle centered at E. It is, then:

$$\ell_{g2} = \text{Arc}\, BC = [BC]\left(\frac{\pi}{3}\right) \tag{2.33}$$

The area of cross section of the flux path is calculated as the average of the stator and rotor area of cross sections and is given as:

$$A_{g2} = \frac{A_{sp2} + A_{rp2}}{2} \tag{2.34}$$

where

$$A_{sp2} = \frac{1}{2}\left(\frac{\beta_s}{4}\frac{D}{2} \cdot L\right) \tag{2.35}$$

$$A_{rp2} = \frac{h_r}{4} L \tag{2.36}$$

2.3.2.2.2 Stator Pole

The length of the flux path is

$$\ell_{sp2} = h_s \tag{2.37}$$

The area of cross section is

$$A_{sp2} = \frac{1}{2}\left(\frac{D}{2}\frac{\beta_s}{4} L\right) \tag{2.38}$$

2.3.2.2.3 Rotor Pole

The length of the flux path is

$$\ell_{rp2} = \frac{h_r}{4} \tag{2.39}$$

The area of cross section is A_{rp2}, given in Eq. (2.36).

2.3.2.2.4 Rotor Back Iron

The length and area of the cross section of the flux path are

$$\ell_{ry2} = \ell_{ry1} \tag{2.40}$$

$$A_{ry2} = A_{ry1} \tag{2.41}$$

as given in the flux path 1 section.

2.3.2.2.5 Stator Back Iron

The length and area of cross section of the flux path are

$$\ell_{sy2} = \ell_{sy1} \tag{2.42}$$

$$A_{sy2} = A_{sy1} \tag{2.43}$$

The Ampere's circuital equation for flux path 2 is written from the magnetic equivalent circuit as:

$$F_2 = [2(R_{sp2} + R_{g2} + R_{rp2}) + (R_{ry2} + R_{sy2})]\phi_2 \tag{2.44}$$

which can be written in terms of flux densities, corresponding magnetic field intensities, and length of the flux paths as:

$$R_{g2} = \frac{\ell_{g2}}{\mu_0 A_{g2}} \tag{2.45}$$

$$R_{sp2} = \frac{H_{sp2}\ell_{sp2}}{B_{sp2}A_{sp2}} \tag{2.46}$$

$$R_{rp2} = \frac{H_{rp2}\ell_{rp2}}{B_{rp2}A_{rp2}} \tag{2.47}$$

$$R_{ry2} = \frac{H_{ry2}\ell_{ry2}}{B_{ry2}A_{ry2}} \tag{2.48}$$

$$R_{sy2} = \frac{H_{sy2}\ell_{sy2}}{B_{sy2}A_{sy2}} \tag{2.49}$$

The error mmf is

$$\Delta F = T_{ph} i - \{2(R_{sp2} + R_{g2} + R_{rp2}) + R_{ry2} + R_{sy2}\}\phi_2 \tag{2.50}$$

which is checked against the error criterion to adjust the stator flux density and to go through the iteration to reduce the mmf error to an acceptable level. The inductance

contributed by flux path 2 is

$$L_{u2} = \frac{2T_{ph}\phi_2}{i} \tag{2.51}$$

where the multiplication factor 2 is inserted as our calculation of ϕ_2 is only for one side of the machine.

From this point on, enlarged figures for flux paths at one set of rotor and stator poles, derivation of the magnetic equivalent circuits, and evaluation of the length and area of the cross section are derived in a manner very similar to that in the previous section.

2.3.2.3 Flux Path 3

The flux path is enlarged and shown in Figure 2.12. The magnetic equivalent circuit is similar to that for flux path 2 and hence not shown here. It is assumed that the flux enters the rotor pole at (h_r/4) from top and leaves the stator pole at $\frac{5}{64}\beta_s$ from the tips. The width of the flux path is over an arc of $\frac{3}{32}\beta_s$ in the stator.

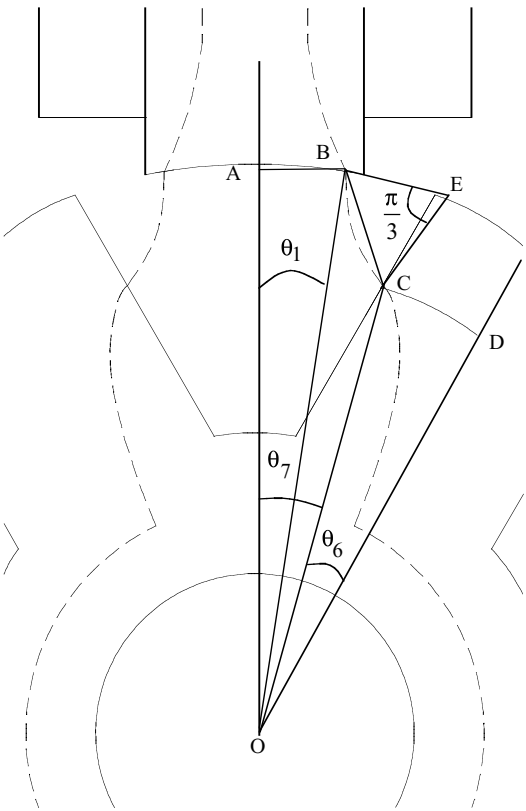

FIGURE 2.12 Flux path 3 at fully unaligned position.

2.3.2.3.1 Air Gap

From Figure 2.12,

$$OD = \left(\frac{D}{2} - \ell_g - \frac{h_r}{4}\right) \tag{2.52}$$

$$CD = \left(\frac{D}{2} - \ell_g\right)\frac{\beta_r}{2} \tag{2.53}$$

$$OB = \frac{D}{2} \tag{2.54}$$

$$\theta_1 = \left(\frac{\beta_s}{2} - \frac{5}{64}\beta_s\right) = \frac{27}{64}\beta_s \tag{2.55}$$

$$\theta_6 = \frac{CD}{OD} \tag{2.56}$$

$$\theta_7 = \theta_{rp} - \theta_6 \tag{2.57}$$

$$\text{coordinates of } B = (x_1, y_1) = [(OB)\sin\theta_1, (OB)\cos\theta_1] \tag{2.58}$$

$$\text{coordinates of } C = (x_2, y_2) = [(OD)\sin\theta_7, (OD)\cos\theta_7] \tag{2.59}$$

$$\text{chord}(BC) = \sqrt{(x_2 - x_1)^2 + (y_2 - y_1)^2} \tag{2.60}$$

$$\ell_{g3} = \text{arc } BC = \text{chord}(BC)\left(\frac{\pi}{3}\right) \tag{2.61}$$

$$A_{g3} = \frac{1}{2}(A_{rp3} + A_{sp3}) \tag{2.62}$$

2.3.2.3.2 Stator Pole

$$\ell_{sp3} \simeq h_s \tag{2.63}$$

$$A_{sp3} = \frac{3}{32}\beta_s\frac{D}{2}L \tag{2.64}$$

2.3.2.3.3 Rotor Pole

$$\ell_{rp3} \simeq \frac{3}{4} h_r \tag{2.65}$$

$$A_{rp3} = \frac{h_r}{4} L \tag{2.66}$$

2.3.2.3.4 Rotor Back Iron

$$\ell_{ry3} \simeq \ell_{ry1} \tag{2.67}$$

$$A_{ry3} \simeq A_{ry1} \tag{2.68}$$

2.3.2.3.5 Stator Back Iron

$$\ell_{sy3} = \ell_{sy1} \tag{2.69}$$

$$A_{sy3} = A_{sy1} \tag{2.70}$$

$$L_{u3} = \frac{T_{ph} \cdot [2\phi_3]}{i} = 2\frac{T_{ph}\phi_3}{i} \tag{2.71}$$

where ϕ_3 is the flux in path 3 for one side of the machine.

2.3.2.4 Flux Path 4

The enlarged flux path nearer one stator and rotor pole is shown in Figure 2.13. The flux leaves the stator at the tips and enters at $(7/8)h_r$ from the rotor pole base. The width of the flux path at the stator pole is assumed to be

$$\left(\frac{\beta_s}{32}\frac{D}{2} + \frac{1}{4}\left(\frac{1}{4}h_s\right)\right)$$

From the figure, the following are derived:

$$\theta_1 = \frac{\beta_s}{2} \tag{2.72}$$

$$\text{coordinates of pole tip } B = (x_3, y_3) = \left[\frac{D}{2}\sin\left(\frac{\beta_s}{2}\right), \frac{D}{2}\cos\left(\frac{\beta_s}{2}\right)\right] \tag{2.73}$$

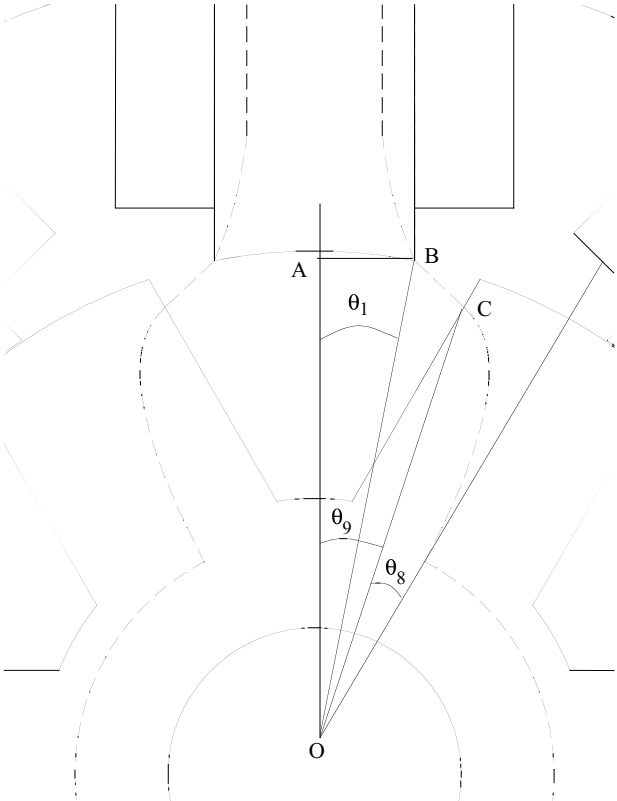

FIGURE 2.13 Flux path 4 in fully unaligned position.

$$OC = \left(\frac{D}{2} - \ell_g - \frac{h_r}{8}\right) \tag{2.74}$$

$$\theta_8 = \frac{\frac{\beta_r}{2}\left(\frac{D}{2} - \ell_g\right)}{\left(\frac{D}{2} - \ell_g - \frac{h_r}{8}\right)} \tag{2.75}$$

$$\theta_9 = \frac{\theta_{rp}}{2} - \theta_8 \tag{2.76}$$

$$\text{coordinates of } C = (x_4, y_4) = [(OC)\sin\theta_9, (OC)\cos\theta_9] \tag{2.77}$$

$$BC = \sqrt{(x_3 - x_4)^2 + (y_3 - y_4)^2} \tag{2.78}$$

2.3.2.4.1 Air Gap

$$\ell_{g4} = BC \tag{2.79}$$

$$A_{g4} = \frac{1}{2}[A_{sp4} + A_{rp4}] \tag{2.80}$$

for which the stator and rotor areas of the cross section for the flux path are given below.

2.3.2.4.2 Stator Pole

$$\ell_{sp4} \simeq h_s \tag{2.81}$$

$$A_{sp4} \simeq \frac{\beta_s}{32}\frac{D}{2}L + \frac{1}{4}\frac{h_s}{4}L \tag{2.82}$$

2.3.2.4.3 Rotor Pole

$$\ell_{rp4} = \frac{7h_r}{8} \tag{2.83}$$

$$A_{rp4} = \frac{h_r}{4}L \tag{2.84}$$

2.3.2.4.4 Rotor Back Iron

$$\ell_{ry4} \simeq \ell_{ry1} \tag{2.85}$$

$$A_{ry4} \simeq A_{ry1} \tag{2.86}$$

2.3.2.4.5 Stator Back Iron

$$\ell_{sy4} = \ell_{sy1} \tag{2.87}$$

$$A_{sy4} = A_{sy1} \tag{2.88}$$

The magnetic equivalent circuit is similar to that of flux path 2. The flux in the path is ϕ_4, hence the inductance contributed by the two flux paths with path 4 is

$$L_{u4} = \frac{2T_{ph}\phi_4}{i} \tag{2.89}$$

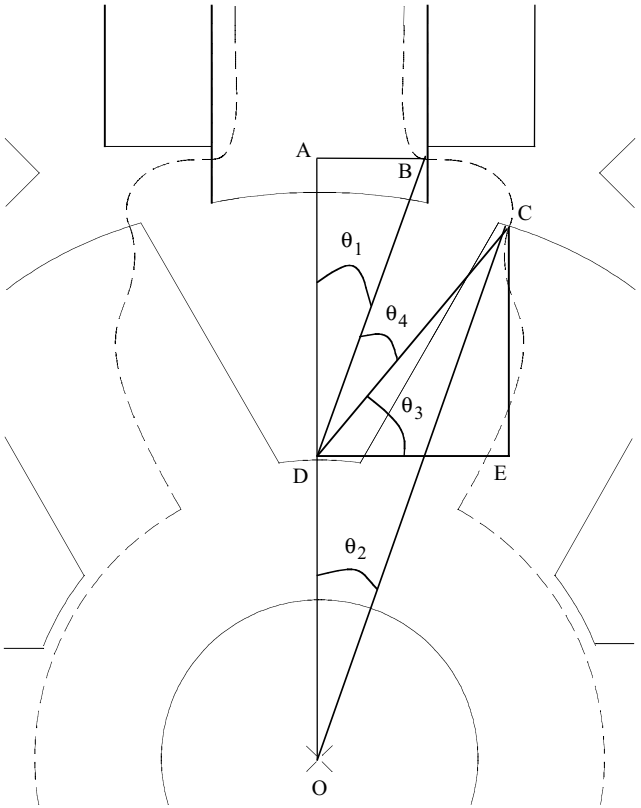

FIGURE 2.14 Flux path 5 in fully unaligned position.

2.3.2.5 Flux Path 5

The flux path has a width of $\frac{3}{4}\left(\frac{h_s}{4}\right)$ on exit at the stator pole and is confined to one eighth of the rotor pole arc on entry. The enlarged flux path is shown in Figure 2.14. The magnetic equivalent circuit is similar to that for flux path 2. From Figure 2.14, the following are derived:

$$x_1 = AB = \frac{D}{2}\sin\left(\frac{\beta_s}{2}\right) \tag{2.90}$$

$$y_1 = OA = \frac{D}{2}\cos\left(\frac{\beta_s}{2}\right) + \frac{5h_s}{32} \tag{2.91}$$

Note that the coordinate is derived at the mean of the flux path that is $(3/16)h_s$ wide but situated above $(1/16)h_s$.

$$\text{coordinates of } B = (x_5, y_5) = \left[\frac{D}{2}\sin\left(\frac{\beta_s}{2}\right), \left\{\frac{D}{2}\cos\left(\frac{\beta_s}{2}\right) + \frac{5h_s}{32}\right\}\right] \tag{2.92}$$

$$\theta_1 = \tan^{-1}\left(\frac{x_5}{AD}\right) = \tan^{-1}\left\{\frac{x_5}{y_5 - \left(\frac{D}{2} - \ell_g - h_r\right)}\right\} \tag{2.93}$$

$$OC = \left(\frac{D}{2} - \ell_g\right) \tag{2.94}$$

$$\theta_2 = \left(\frac{\theta_{rp}}{2} - \frac{7}{16}\beta_r\right) \tag{2.95}$$

$$\text{coordinates of } C = (x_6, y_6) = [(OC)\sin\theta_2, (OC)\cos\theta_2] \tag{2.96}$$

$$\text{coordinates of } D = (x_7, y_7) = \left[0, \left(\frac{D}{2} - \ell_g - h_r\right)\right] \tag{2.97}$$

$$DC = \sqrt{(x_7 - x_6)^2 + (y_7 - y_6)^2} \tag{2.98}$$

$$DB = \sqrt{(x_7 - x_5)^2 + (y_7 - y_5)^2} \tag{2.99}$$

$$\theta_3 = \tan^{-1}\left(\frac{CE}{DE}\right) = \tan^{-1}\left(\frac{y_6 - y_7}{x_6}\right) \tag{2.100}$$

$$\theta_4 = \frac{\pi}{2} - \theta_3 - \theta_1 \tag{2.101}$$

2.3.2.5.1 Air Gap

The length of flux path 5 in the air gap can be approximated as the arc of a circle with an average radius of DB and DC and subtended by θ_4 as:

$$\ell_{g5} = \frac{1}{2}(DB + DC)\theta_4 \tag{2.102}$$

The area of cross section is the mean of the stator and rotor pole cross sections encountered by the flux path and is given as:

$$A_{g5} = \frac{1}{2}(A_{sp5} + A_{rp5}) \tag{2.103}$$

2.3.2.5.2 Stator Pole

$$\ell_{sp5} \cong h_s \tag{2.104}$$

$$A_{sp5} = \frac{3}{4}\frac{h_s}{4}L \tag{2.105}$$

2.3.2.5.3 Rotor Pole

$$\ell_{rp5} = h_r \tag{2.106}$$

$$A_{rp5} = \left(\frac{D}{2} - \ell_g\right)\frac{\beta_r}{8}L \tag{2.107}$$

2.3.2.5.4 Rotor Back Iron

$$\ell_{ry5} = \ell_{ry1} \tag{2.108}$$

$$A_{ry5} = A_{ry1} \tag{2.109}$$

2.3.2.5.5 Stator Back Iron

$$\ell_{sy5} = \ell_{sy1} \tag{2.110}$$

$$A_{sy5} = A_{sy1} \tag{2.111}$$

The inductance contributed by the flux in path 5 is

$$L_{u5} = 2\frac{T_{ph}\phi_5}{i} \tag{2.112}$$

where ϕ_5 is the flux in path 5.

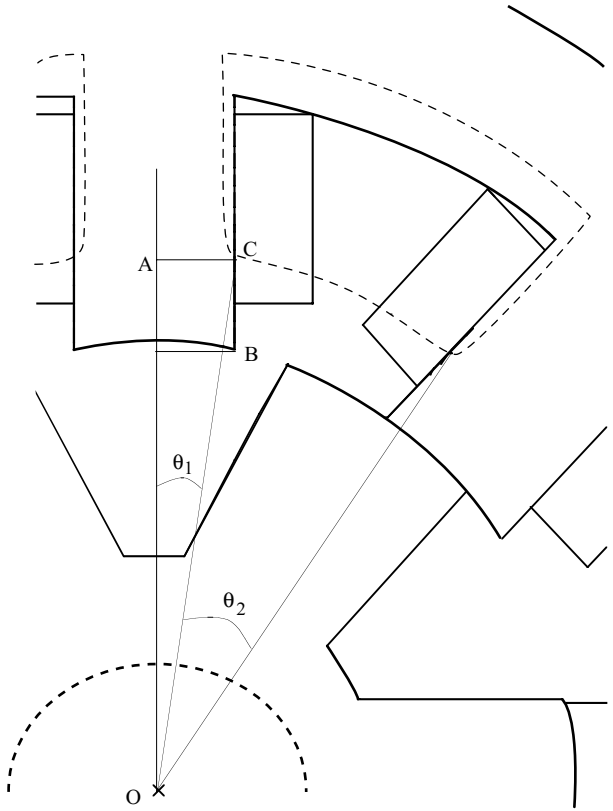

FIGURE 2.15 Flux path 6 in fully unaligned position.

2.3.2.6 Flux Path 6

Flux path 6 is shown in detail in Figure 2.15. The flux path can be assumed to be an arc centered at the center of the shaft. The flux path is $(h_s/4)$ wide and is at a height of $\left(\frac{h_s}{4}+\frac{1}{2}\frac{h_s}{4}\right)$. The coordinates of OC are

$$y_1 = OA = \frac{D}{2}\cos\left(\frac{\beta_s}{2}\right)+\frac{3h_s}{8} \tag{2.113}$$

$$x_1 = AC = \frac{D}{2}\sin\left(\frac{\beta_s}{2}\right) \tag{2.114}$$

and θ_1 is

$$\theta_1 = \sin^{-1}\left(\frac{x_1}{\sqrt{(x_1^2+y_1^2)}}\right) \tag{2.115}$$

θ_2 is obtained as:

$$\theta_2 = \left(\frac{2\pi}{P_s} - 2\theta_1\right) \tag{2.116}$$

where P_s is the number of stator poles.

2.3.2.6.1 Air Gap

The length of the air gap for flux path 6 is

$$\ell_{g6} = (OC)\theta_2 = \left[\sqrt{(x_1^2 + y_1^2)}\right]\theta_2 \tag{2.117}$$

The area of the cross section for the flux path is

$$A_{g6} = \frac{1}{2}[A_{sp6} + A_{rp6}] \tag{2.118}$$

2.3.2.6.2 Stator Pole

The length of the flux path in stator pole is approximated as:

$$\ell_{sp6} \simeq \frac{5}{8} h_s \tag{2.119}$$

$$A_{sp6} = \frac{h_s}{4} L \tag{2.120}$$

2.3.2.6.3 Stator Back Iron

The length and area of the cross section are

$$\ell_{sy6} \simeq \left(\frac{D}{2} + h_s + \frac{b_{sy}}{4}\right)\left[\frac{2\pi}{P_s} - 2\theta_1\right] \tag{2.121}$$

$$A_{sy6} \simeq A_{sy1} \tag{2.122}$$

2.3.2.6.4 Magnetic Equivalent Circuit

The magnetic equivalent circuit for flux path 6 contains reluctances due to the stator poles, air gap, and stator back iron as shown in Figure 2.16. It is noted that there are four flux paths 6 in this machine. The flux in them encloses only three eighths of the stator turns. The flux in path 6 is

$$\phi_6 = \frac{F_6}{2R_{sp6} + R_{g6} + R_{sy6}} = \frac{\frac{3}{8}(T_{ph} i)}{2R_{sp6} + R_{g6} + R_{sy6}} \tag{2.123}$$

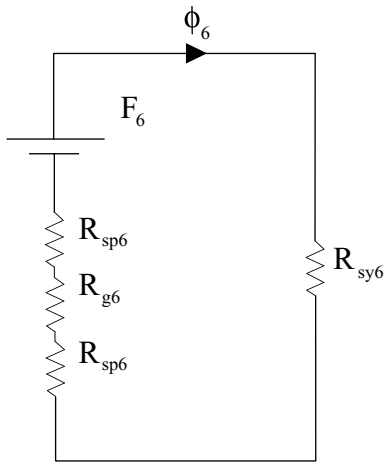

FIGURE 2.16 Magnetic equivalent circuit for flux path 6.

The inductance contributed by the flux path 6 is

$$L_{u6} = \frac{4\left\{\frac{3}{8}(T_{ph}\phi_6)\right\}}{i} \tag{2.124}$$

as there are four paths of path 6.

2.3.2.7 Flux Path 7

An enlarged flux path 7 is shown in Figure 2.17, and its magnetic equivalent circuit for one path is shown in Figure 2.18. For the calculation of flux path length, the flux path is centered at B with a radius of $(h_s/4)$ and an angle of $(\pi/2)$. Various lengths of the pole, air gap, and back iron segments are

$$\ell_{sy7} \simeq \frac{h_s}{4} + \frac{b_{sy}}{4} \tag{2.125}$$

$$\ell_{g7} \simeq \frac{h_s}{4}\frac{\pi}{2} \tag{2.126}$$

$$\ell_{sy7} \simeq \frac{h_s}{4} \tag{2.127}$$

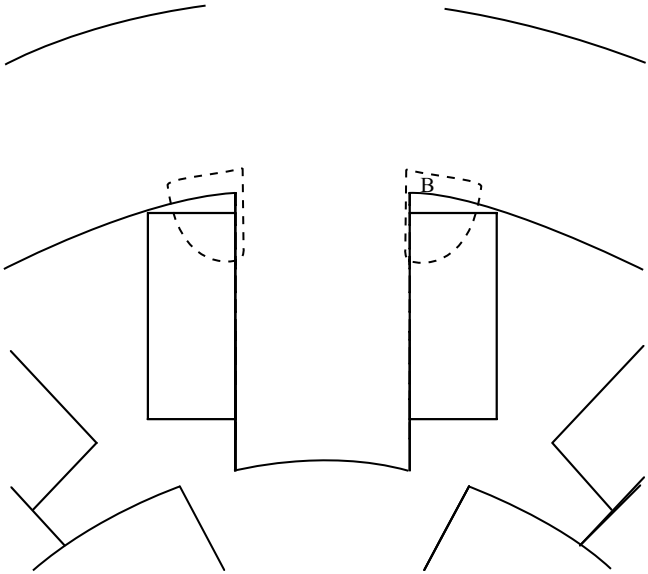

FIGURE 2.17 Flux path 7 in fully unaligned position.

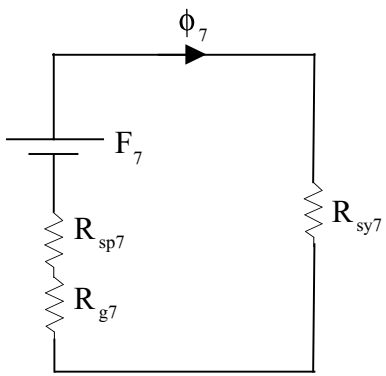

FIGURE 2.18 Magnetic equivalent circuit for flux path 7.

The areas of cross section for the segments are

$$A_{sp7} = \frac{h_s}{2} L \tag{2.128}$$

$$A_{g7} = A_{sp7} \tag{2.129}$$

$$A_{sy7} = A_{sy1} \tag{2.130}$$

The flux in path 7 is ϕ_7; the mmf causing this is F_7 and is equal to one fourth of the per-phase mmf, $T_{ph}i$. The inductance contributed by the four flux paths 7 is

$$L_{u7} = 4\frac{T_{ph}}{2}\frac{\phi_7}{i} = \frac{2T_{ph}\phi_7}{i} \tag{2.131}$$

2.3.2.7.1 *Unaligned Inductance*

The unaligned inductance is obtained by the sum of all the inductances contributed by the flux paths and it is given by:

$$L_u = \sum_{j=1}^{7} L_{uj} \tag{2.132}$$

2.3.3 Aligned Inductance

The derivation of inductance is much simpler for the stator and rotor pole aligned positions than for unaligned positions. The flux lines, about 90 to 98%, pass the air gap between the stator and rotor. There is a small flux due to leakage between adjacent poles. The fringing is not very significant and can be accounted for, if necessary. For example, consider the flux plot of the 8/6 machine considered for illustration in the derivations and shown in Figure 2.19. The flux in the machine consists of flux path 1 and flux path 7, identified for the unaligned position. Flux path 1 consists of the majority of the flux and is mutual flux connecting the stator and rotor.

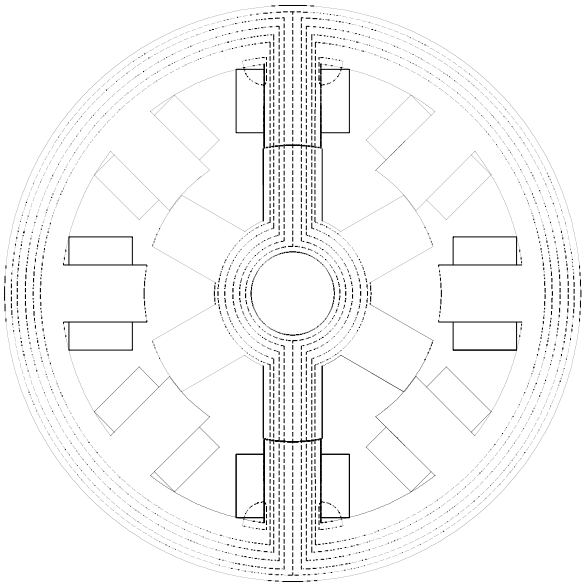

FIGURE 2.19 Flux paths at fully aligned position.

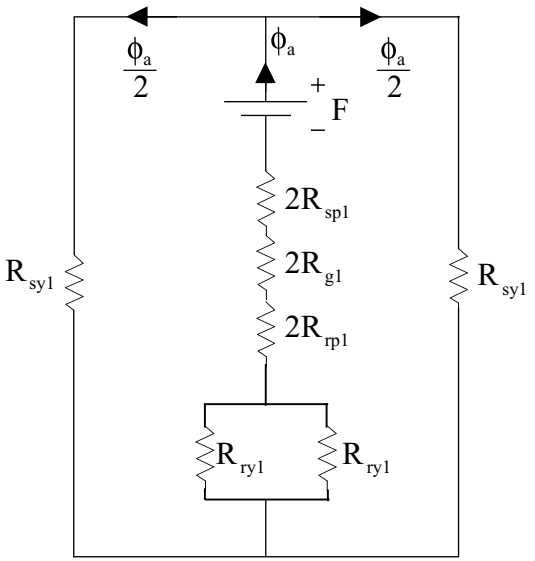

FIGURE 2.20 Magnetic equivalent circuit for aligned position.

Flux path 7 has leakage flux only when connecting the excited poles with adjacent poles and carries only a small flux. The derivations for these two flux paths are given separately.

2.3.3.1 Flux Path 1

For the sake of simplicity, the magnetic equivalent circuit of the SRM at the aligned position can be deduced and shown in Figure 2.20, for mutual flux path 1. The derivations for the length and area of cross section of the mutual flux path (i.e., flux path 1) are given in Table 2.1.

Applying Ampere's circuital law, mmf calculated for each path are summed and given as:

$$F_c = 2[H_{sp1}\ell_{sp1} + H_{g1}\ell_{g1} + H_{rp1}\ell_{rp1}] + H_{ry1}\ell_{ry1} + H_{sy1}\ell_{sy1} \tag{2.133}$$

The magnetic field intensities are extracted from the B-H characteristics using the flux densities calculated in parts of the machine. From the calculated and applied mmf, the error mmf is found as:

$$\Delta F = F - F_c = T_{ph}i - F_c \tag{2.134}$$

It is reduced by iteration as described earlier. The flux in flux path 1 is found as:

$$\phi_a = \frac{T_{ph}i}{2[R_{sp1} + R_{g1} + 2R_{p1}] + \frac{1}{2}R_{y1} + \frac{1}{2}R_{sy1}} \tag{2.135}$$

TABLE 2.1
Length and Area of Cross Section of Flux Path 1 in the Aligned Position

Segment	Path Length	Area of Cross Section of Flux Path
Air gap	$\ell_{g1} = \ell_g$	$A_{g1} = \dfrac{\beta_s \frac{D}{2} L + \beta_r (\frac{D}{2} - \ell_g) L}{2}$
Stator pole	$\ell_{sp1} = h_s$	$A_{sp} = \beta_s \dfrac{D}{2} L$
Rotor pole	$\ell_{rp1} = h_r$	$A_{rp1} = \beta_r \left(\dfrac{D}{2} - \ell_g\right) L$
Rotor back iron	$\ell_{ry1} = \dfrac{\pi}{2}\left[\dfrac{D}{4} - \ell_g - h_r + \dfrac{D_{sh}}{2}\right]$	$A_{ry1} = \left(\dfrac{D}{2} - \ell_g - h_r\right) L$
Stator back iron	$\ell_{sy1} = \dfrac{\pi}{2}[D + h_s + b_{sy}]$	$A_{sy1} = b_{sy} L$

TABLE 2.2
Length and Area of Cross Section of Flux Path 7 in the Aligned Position

Segment	Path Length	Area of Cross Section
Air gap	$\ell_{g7} = \dfrac{3h_s}{4} \dfrac{\pi}{2}$	$A_{g7} = \dfrac{3h_s}{4} L$
Stator pole	$\ell_{sp7} = \dfrac{1}{2} \dfrac{3h_s}{4} + \dfrac{b_{sy}}{2}$	$A_{sp7} = \dfrac{1}{2}\left[\dfrac{3h_s}{4} L\right]$
Stator back iron	$\ell_{sy7} \simeq \ell_{sp7}$	$A_{sy7} = b_{sy} L$

And this flux contributes an inductance,

$$L_{a1} = \frac{T_{ph} \phi_a}{i} \tag{2.136}$$

2.3.3.2 Flux Path 7

For leakage flux path 7, the length and area of the cross sections of various parts in the flux path are derived similarly and given in Table 2.2. The magnetic equivalent circuit for this flux path is the same as that for the fully unaligned position given earlier. The circuital equation is

$$F_c = [H_{sp7} \ell_{sp7} + H_{g7} \ell_{g7} + H_{sy7} \ell_{sy7}] \tag{2.137}$$

and the mmf error for this calculated value is derived as:

$$\Delta F = \frac{3}{4} T_{ph} i - F_c \tag{2.138}$$

as only three quarters of the stator mmf are involved with this flux path.

The flux in this path is derived as:

$$\phi_{7a} = \frac{\frac{3}{4} T_{ph} i}{R_{sp7} + R_{g7} + R_{sy7}} \tag{2.139}$$

and the inductance due to four flux paths in path 7 is

$$L_{a7} = 4\left[\frac{\frac{3}{4} T_{ph} i}{i}\right] = \frac{3 T_{ph} \phi_{7a}}{i_a} \tag{2.140}$$

Total aligned inductance is then obtained as:

$$L_a = L_{a1} + L_{a7} \tag{2.141}$$

2.3.4 Results and Comparison

The validity of similar analytical procedures for predicting aligned and unaligned inductances is evaluated by comparing finite element analysis results and measurements obtained from a prototype 6/4-pole SRM for which the details are given below:

Number of stator poles	6
Number of rotor poles	4
Stator diameter (outer)	19 cm
Rotor diameter (bore)	10.206 cm
Core length	6.037 cm
Air gap	0.025 cm
Back iron thickness	1.0515 cm
Stator pole arc	0.418 rad
Rotor pole arc	0.628 rad
Turns per phase	536
Wire size	AWG #19
Core material	M19 steel

The comparison is made for three currents, and the base value for the current is the prototype's rated current of 10A. This makes the range of observations from 0.1 to 2 p.u. sufficient for a reasonable comparison (see Table 2.3). The analytical results are closer to the measurements than the results of the finite element method.

TABLE 2.3
Comparison of Inductance by Various Methods

Phase Current (I_p, A)	Unaligned Inductance (L_u, mH)			Aligned Inductance (L_a, mH)			Average Electromagnetic Torque (N · m)		
	Analytical	FEM[a]	Measured	Analytical	FEM[a]	Measured	Analytical	FEM[a]	Measured
1	23.2	25.8	35.5	923	843	879	0.88	0.80	0.90
10	28.3	25.8	40.7	130	133	155	18.77	18.50	20.30
20	29.5	25.8	35.6	82.4	75.5	89	38.60	37.80	41.60

[a] FEM = finite element method.

The close correlation, however, between the analytical and experimental results validates the magnetic circuit approach and derivations.

A second machine with 8/6 poles is considered for verifying the algorithm developed for predicting aligned and unaligned inductances, for which the details are given below:

Number of stator poles	8
Number of rotor poles	6
Power output	5 hp
Stator pole arc	18 degrees
Rotor pole arc	22 degrees
Air gap length	0.5 mm
Outer stator diameter	190 mm
Bore diameter	100.6 mm
Stack length	200 mm
Shaft diameter	28 mm
Speed	1500 rpm
Stator back iron thickness	12 mm
Height of stator pole	32.7 mm
Height of rotor pole	19.8 mm
Turns per phase	154
Conductor area of cross section	1.588 mm^2
Rated current	13A
Lamination material	M43

Comparison between finite element analysis and analytical results for the 8/6-SRM at the rated current is given in the following table:

	Finite Element Analysis (mH)	Analytical (mH)
Aligned inductance	65.41	66.79
Unaligned inductance	11.35	11.38

The close correlation at the rated (nominal) current for this machine validates the method.

2.3.5 Performance Evaluation

Having determined the aligned and unaligned inductances as a function of excitation current, an approximate output capability of the machine can be found. It requires some approximations, such as:

1. The phase inductance variation is linear from the initial overlap to full overlap positions of the stator and rotor poles. The beginning of the overlap of the stator and rotor poles is given by:

$$\theta_i = \frac{\pi}{P_r} - \left(\frac{\beta_s + \beta_r}{2}\right) = \frac{\theta_{rp} - (\beta_s + \beta_r)}{2} \tag{2.142}$$

   The full overlap position is given by:

$$\theta_o = \frac{\theta_{rp}}{2} \tag{2.143}$$

   where the initial and full overlap are measured from the fully unaligned position.
2. The phase inductance at the initial overlap position is equal to the phase inductance at the unaligned position.

Then, for a given excitation, the aligned and unaligned flux linkages vs. excitation current are obtained by the product of the inductance with the excitation current. From the area enclosed between the aligned and unaligned flux linkages vs. excitation current characteristics, the work done and torque can be evaluated.

This is very approximate, as most of the time in a variable-speed SRM drive current injection up to the full alignment position at a constant excitation level is rare, as issues such as advance commutation of current arise to avoid operation in the regeneration mode and torque ripple minimization require current programming as a function of rotor position (discussed in Chapter 5).

Variable current vs. rotor position and variable on times with variable phase displacement of the current with respect to fully unaligned and aligned positions are required to deliver desired performance. The performance computation requires the complete set of flux linkages or inductance vs. rotor position vs. excitation current. Such a set of characteristics can be analytically derived by using the procedure developed for fully unaligned and aligned inductance computations. A few intermediate positions between completely unaligned and aligned can be chosen and the characteristics computed. Then the inductance between two computed positions can be extrapolated to obtain the inductances for intermediate positions. The accuracy in the case may be compromised when the inductance at only a few intermediate positions are known. An alternative method is to derive the analytic relationships of various flux paths as a function of rotor position, in which case extrapolation of inductances is avoided and computation of inductances is carried out for any desired rotor position and excitation current. The latter method is chosen here and derivations are made and presented in the next section.

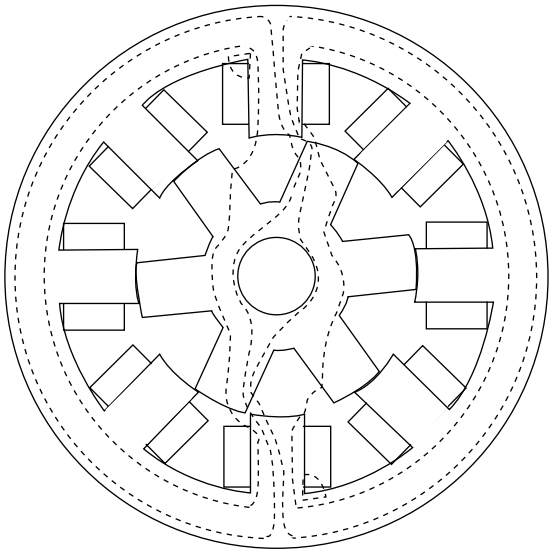

FIGURE 2.21 Flux distribution in region 1.

2.3.6 Inductances at Intermediate Positions

Within the intermediate position between completely unaligned and aligned stator and rotor poles, there are two distinct regions in which the flux patterns change in the machine: from the fully unaligned position to initial overlap of the stator and rotor poles (region 1) and from the initial overlap to complete overlap of the stator and rotor poles (region 2). Sample flux maps for each of these regions are shown in Figures 2.21 and 2.22, respectively.

When the poles start barely overlapping (i.e., region 1), the flux is diverted entirely to the closer rotor pole and the leakage flux path starts to increase at the base of the stator pole on one side. In overlapping region 2, the flux density increases in the stator poles and the leakage flux path increases resulting in the leakage flux connecting the adjacent stator poles on either side. This leakage flux path variation is difficult to predict with the magnetic equivalent circuit approach; therefore, it will be included by one simple path at the base of the excited stator poles.

2.3.6.1 Region 1

The region 1 is defined by:

$$0 \le \theta \le \left(\frac{\theta_{rp} - (\beta_r + \beta_s)}{2} \right) \tag{2.144}$$

Only the flux paths, including leakage, are considered for illustration (see Figure 2.23), for region 1. Paths 1 to 5 are for mutual flux and path 6 is for leakage flux at the base of the excited stator poles. The flux paths in the stator back iron and rotor body

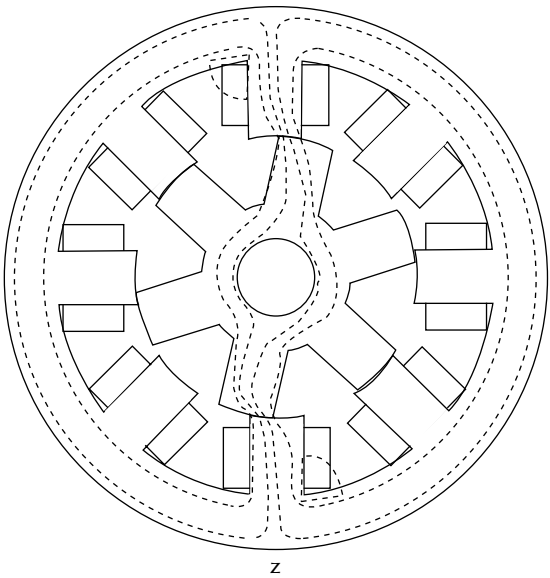

FIGURE 2.22 Flux distribution in region 2.

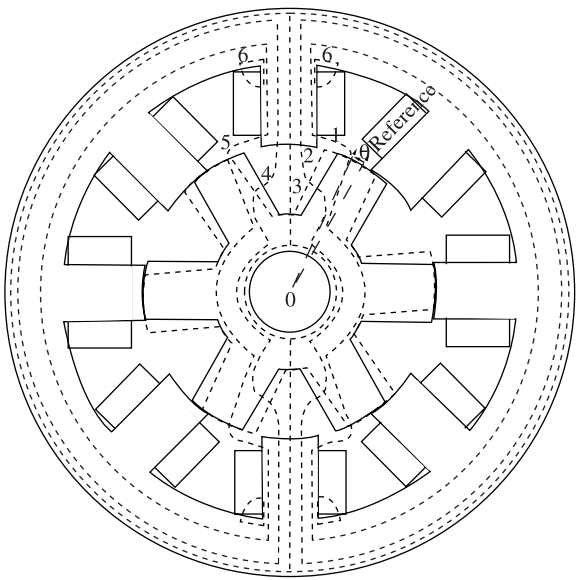

FIGURE 2.23 Flux distribution in region 1.

are very similar to those of the aligned and unaligned position flux maps, so they are not shown in the figure. Derivations for path 6 have been made in the aligned inductance section. It is assumed here that flux path 6 is independent of rotor position; therefore, only derivations for flux paths 1 to 5 as a function of rotor position are developed in the following section.

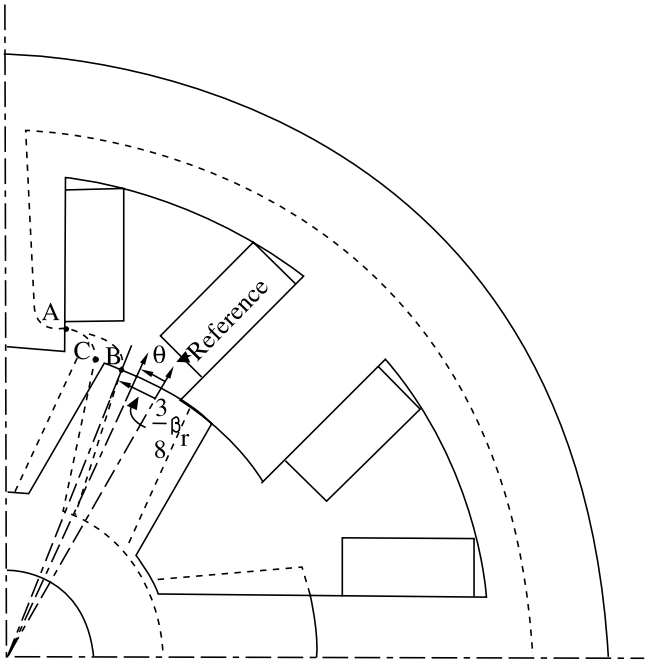

FIGURE 2.24 Flux path 1 in region 1.

2.3.6.1.1 Flux Path 1

The flux path in the air gap is enlarged and shown in Figure 2.24. The mean flux line leaves the stator pole at one eighth of the stator pole height from the air gap, denoted by point A, and enters the rotor pole at $(1/8)\beta_r$ from its leading edge. Even though only one flux line is shown, the width of this flux path is one quarter of the stator pole height and, therefore, is centered around $(1/8)h_s$. The length of the flux path is given by the arc AB at the fully unaligned position. As the rotor is moved by θ, its length is given by arc AC. The key to obtaining the inductance contributed by this path is to formulate the length of flux path 1 in the air gap as a function of rotor position and machine dimensions. Note also that there is no symmetry of flux path 1 as seen from the upper stator pole and its diametric opposite pole at the lower side. This needs to be considered for calculation of the length of flux path 1 in the air between the stator and rotor poles at both the upper and lower poles. The corresponding values will be indicated by subscripts u and ℓ. It is derived as follows with other relevant parameters to compute the reluctance.

The linear distance between A and C is found by finding their coordinates with the origin, O, at the center of the shaft. Then, the arc AC is found by making an equilateral triangle with length AC. From that arc AC is evaluated. The steps are

$$\text{coordinates of } O = (0, 0) \tag{2.145}$$

$$\text{coordinates of } A = (x_1, y_1) \tag{2.146}$$

where

$$x_1 = \frac{D}{2}\sin\left(\frac{\beta_s}{2}\right) \tag{2.147}$$

$$y_1 = \frac{D}{2}\cos\frac{\beta_s}{2} + \frac{h_s}{8} \tag{2.148}$$

$$\text{coordinates of } C = (x_2, y_2) \tag{2.149}$$

where

$$x_2(\theta) = \left(\frac{D}{2} - \ell_g\right)\sin\left(\frac{\theta_{rp}}{2} - \frac{1}{8}\beta_r - \theta\right) \tag{2.150}$$

$$y_2(\theta) = \left(\frac{D}{2} - \ell_g\right)\cos\left(\frac{\theta_{rp}}{2} - \frac{1}{8}\beta_r - \theta\right) \tag{2.151}$$

Note that x_2 and y_2 have been expressed as a function of rotor position, θ. From the coordinates of A and C, the distance between A and C is calculated as:

$$AC = \sqrt{(x_2 - x_1)^2 + (y_2 - y_1)^2} \tag{2.152}$$

Then, the arc AC may be thought of as the air gap at the upper pole and approximated in terms of the chord AC as:

$$\ell_{g1u} = \text{arc } AC = AC \cdot \left(\frac{\pi}{3}\right) \tag{2.153}$$

Similarly, the length of the mean flux line in path 1 at the lower pole is evaluated by:

$$x_3 = \left(\frac{D}{2} - \ell_g\right)\sin\left(\frac{\theta_{rp}}{2} - \frac{1}{8}\beta_r + \theta\right) = x_2(-\theta) \tag{2.154}$$

$$y_3 = \left(\frac{D}{2} - \ell_g\right)\cos\left(\frac{\theta_{rp}}{2} - \frac{1}{8}\beta_r + \theta\right) = y_2(-\theta) \tag{2.155}$$

$$\ell_{g1\ell} = \frac{\pi}{3} \cdot \sqrt{(x_3 - x_1)^2 + (y_3 - y_1)^2} \tag{2.156}$$

Therefore, the total length of flux path 1 in air at the lower side is

$$\ell_{g1} = \ell_{g1u} + \ell_{g1\ell} \tag{2.157}$$

The area of the flux path in the air gap is

$$A_{g1} = \left[\frac{h_s}{4} + \frac{1}{4}\beta_r\left(\frac{D}{2} - \ell_g\right)\right]\frac{L}{2} \tag{2.158}$$

Similarly, the length and area of the core section of the flux path in the stator poles, rotor poles, and stator and rotor back iron are derived and given below:

1. **Stator pole:** For both stator poles,

$$\ell_{sp1} = 2\frac{7}{8}h_s \tag{2.159}$$

$$A_{sp1} = \frac{h_s L}{4} \tag{2.160}$$

2. **Rotor pole:** For both rotor poles,

$$\ell_{rp1} = 2h_r \tag{2.161}$$

$$A_{rp1} = \frac{\beta_r}{4}\left(\frac{D}{2} - \ell_g\right)L \tag{2.162}$$

3. **Stator back iron:**

$$\ell_{sy1} = \pi\left(\frac{D}{2} + h_s + \frac{b_{sy}}{2}\right) \tag{2.163}$$

$$A_{sy1} = b_{sy}L \tag{2.164}$$

4. **Rotor back iron:**

$$\ell_{ry1} = \frac{\pi}{2}\left(\frac{D}{2} - \ell_g - h_r - \frac{D_{sh}}{2}\right) \tag{2.165}$$

$$A_{ry1} = \left(\frac{D}{2} - \ell_g - h_r - \frac{D_{sh}}{2}\right)L \tag{2.166}$$

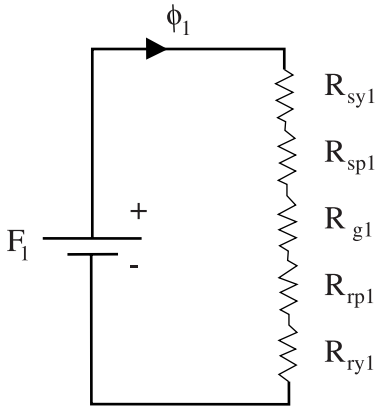

FIGURE 2.25 Magnetic equivalent circuit for flux path 1 in region 1.

The magnetic equivalent circuit is shown in Figure 2.25, where the excitation mmf is given by:

$$F_1 = T_{ph} i \tag{2.167}$$

The total stator pole reluctance is computed for both the flux paths as:

$$R_{sp1} = \frac{\ell_{sp1}}{\mu_o \mu_{r1} A_{sp1}} \tag{2.168}$$

where μ_{r1} is the relative permeability in the stator pole. Similarly, for both rotor pole paths, the reluctance is

$$R_{rp1} = \frac{\ell_{rp1}}{\mu_o \mu_{r2} A_{rp1}} \tag{2.169}$$

where μ_{r2} is the relative permeability in the rotor pole. The stator and rotor back iron reluctances, respectively, for path 1 are

$$R_{sy1} = \frac{\ell_{sy1}}{\mu_o \mu_{r3} A_{sy1}} \tag{2.170}$$

$$R_{ry1} = \frac{\ell_{ry1}}{\mu_o \mu_{r4} A_{ry1}} \tag{2.171}$$

where μ_{r3} and μ_{r4} are relative permeabilities for the stator and rotor back iron, respectively. The reluctance of flux path 1 for both air gaps combined is

$$R_{g1} = \frac{\ell_{g1}}{\mu_o A_{g1}} \tag{2.172}$$

The procedure to calculate the stator flux density and all other variables of interest are very much similar to the procedure developed in the previous section; therefore, for the sake of brevity, it will not be repeated here. The inductance contributed by the flux path for the considered rotor position, θ, is

$$L_1 = \frac{T_{ph}\phi_1(\theta)}{i} \tag{2.173}$$

where $\phi_1(\theta)$ is the flux in path 1.

2.3.6.1.2 Flux Path 2

This flux path is subtended by one-fifth stator pole arc and it crosses to the rotor pole from its side with a width of $(1/3)h_r$ at a height of $(1/4)h_r$ (see Figure 2.23). As for its flow to the diametrically opposite rotor pole and then to the diametrically opposite stator pole, it is identical to the upper part just described. The stator back iron on the right-hand side carries the flux in path 2. Flux path 2 enlarged for the upper part is shown in Figure 2.26. Note the similarity of the flux path in the lower part of the stator and rotor poles as this flux passes through the diametrically opposite rotor pole. The relevant lengths of the mean flux lines and the area of cross section of the flux paths are derived similar to the procedure developed in the previous section. The steps involved for the path in the air gap are

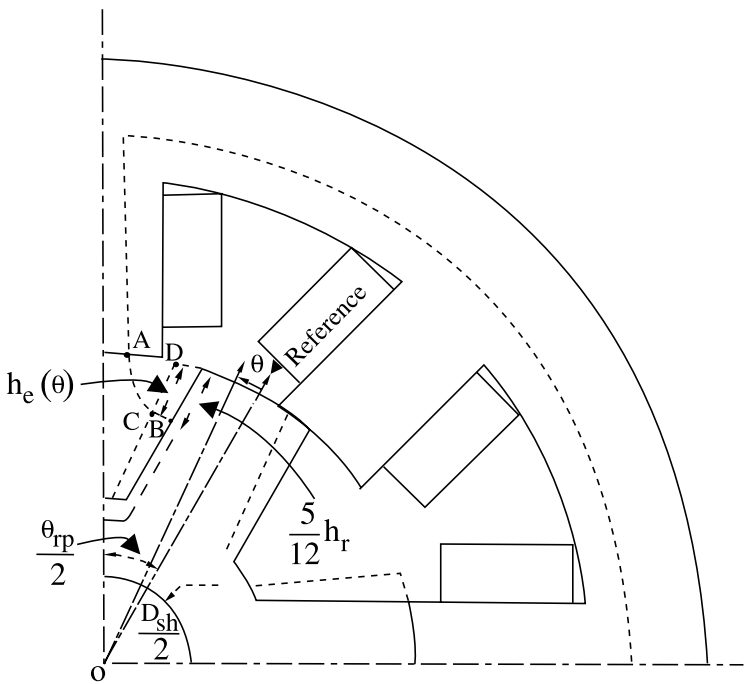

FIGURE 2.26 Flux path 2 in region 1.

For the coordinates of $A = (x_1, y_1)$,

$$x_1 = \frac{D}{2}\sin\left(\frac{\beta_s}{5}\right) \tag{2.174}$$

$$y_1 = \frac{D}{2}\cos\left(\frac{\beta_s}{5}\right) \tag{2.175}$$

$$\text{coordinates of } C = (x_2, y_2) \tag{2.176}$$

$$x_2(\theta) = \left(\frac{D}{2} - \ell_g - h_{eu}(\theta)\right)\sin\left(\frac{\theta_{eu}}{2} - \frac{\beta_r}{2} - \theta\right) \tag{2.177}$$

$$y_2(\theta) = \left(\frac{D}{2} - \ell_g - h_{eu}(\theta)\right)\cos\left(\frac{\theta_{rp}}{2} - \frac{\beta_r}{2} - \theta\right) \tag{2.178}$$

$$AC = \sqrt{(x_2 - x_1)^2 + (y_2 - y_1)^2} \tag{2.179}$$

$$\ell_{g2u} \simeq \frac{\pi}{3} \cdot AC \tag{2.180}$$

where the height, $h_{eu}(\theta)$, at which the flux enters the side of the rotor pole as it draws to the end of region 1, becomes half its original height at unalignment. It can be approximately represented as:

$$h_{eu}(\theta) = \frac{5}{12}h_r\left(1 - \frac{\theta}{2\left(\frac{\theta_{rp}}{2} - \frac{\beta_s + \beta_r}{2}\right)}\right) \tag{2.181}$$

The length of the flux path in the air between the lower stator and rotor poles is

$$\ell_{g2\ell} = \sqrt{(x_3 - x_1)^2 + (y_3 - y_1)^2} \tag{2.182}$$

where x_1 and y_1 are given by Eqs. (2.174) and (2.175), respectively, and x_3 and y_3 are derived by modifying Eqs. (2.177) and (2.178) in the section on flux path 2:

$$x_3(\theta) = \left(\frac{D}{2} - \ell_g - h_{e\ell}(\theta)\right)\sin\left(\frac{\theta_{rp}}{2} - \frac{\beta_r}{2} + \theta\right) \tag{2.183}$$

$$y_3(\theta) = \left(\frac{D}{2} - \ell_g - h_{e\ell}(\theta)\right)\cos\left(\frac{\theta_{rp}}{2} - \frac{\beta_r}{2} + \theta\right) \tag{2.184}$$

$$h_{e\ell}(\theta) = \frac{5}{12}h_r\left(1 + \frac{\theta}{2\left(\frac{\theta_{rp} - (\beta_s + \beta_r)}{2}\right)}\right) = h_{eu}(-\theta) \tag{2.185}$$

The total mean length of the flux lines in the air then is

$$\ell_{g2} = \ell_{g2u} + \ell_{g2\ell} \tag{2.186}$$

The length of the flux path in rotor pole is

$$\ell_{rp2u} = h_r - h_{eu}(\theta) \tag{2.187}$$

$$\ell_{rp2\ell} = h_r - h_{e\ell}(\theta) \tag{2.188}$$

The total length of flux line in rotor pole is

$$\ell_{rp2} = \ell_{rp2u} + \ell_{rp2\ell} \tag{2.189}$$

The area of cross section of the flux path in the air is the average of the stator and rotor pole areas of cross section and is given as:

$$A_{g2} = \left(\frac{\beta_s}{5}\frac{D}{2} + \frac{1}{3}h_r\right)\frac{L}{2} \tag{2.190}$$

All other values are straightforward and are not elaborated here. The magnetic equivalent circuit is identical to that of path 1 shown in Figure 2.26.

2.3.6.1.3 Flux Path 3

Flux from one fifth of the stator pole arc flows into the rotor interpolar space, the mean of which is indicated by the line *AB* at the center of the stator pole in Figure 2.27. It is so until the rotor interpolar space moves away or a short air path to the side of the rotor pole emerges. The latter case arises only in region 2 and never in region 1; therefore, two cases arise for flux path 3. When rotor pole movement is less than half, the interpolar arc is given as:

$$\theta \le \frac{\theta_{rp} - \beta_r}{2}$$

in which case, the flux path is in the air and is indicated by *AB*. Then, the mean length of flux path 3 in the air for the upper and lower parts is

$$\ell_{g3u} = AB = \left(\frac{D}{2} - \ell_g - h_r\right) = \ell_{g3\ell} \tag{2.191}$$

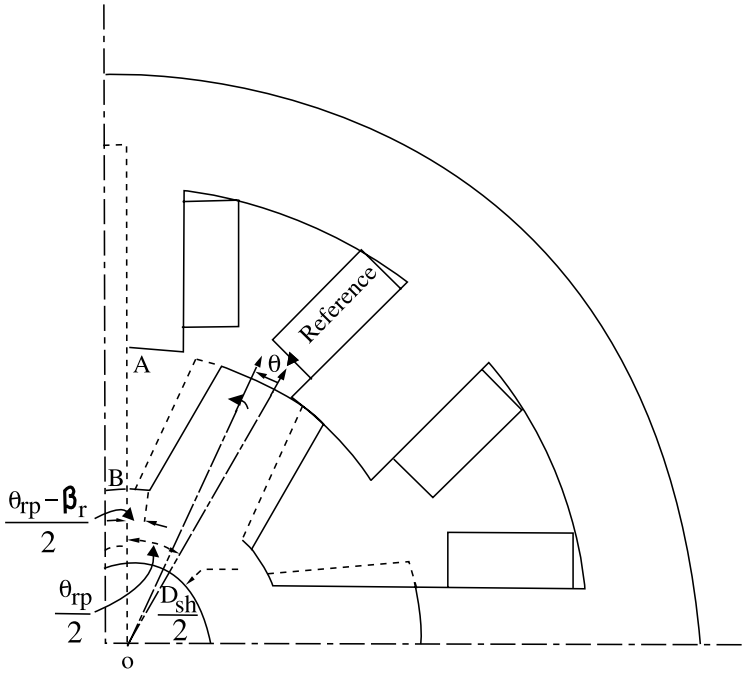

FIGURE 2.27 Flux path 3 in region 1.

Hence, the total air length in path 3 is

$$\ell_{g3} = \ell_{g3u} + \ell_{g3\ell} = 2(AB) = 2\left(\frac{D}{2} - \ell_g - h_r\right) \tag{2.192}$$

It is tacitly assumed that a path to the leading side of the rotor pole is greater than AB and is not considered. Such an assumption is very valid in practice.

Note that the upper and lower stator and rotor pole paths are similar and the equivalent circuit is identical to that for flux path 1 shown in Figure 2.25. The area of cross section of flux path 3 in the air is

$$A_{g3} = \frac{1}{5}\beta_s \frac{D}{2} L \tag{2.193}$$

in region 1. The air gap area is considered equal to the stator pole area for flux path 3, as the flux path is straight and does not warrant consideration like other paths. All other variables for other parts of the machine are easy to derive and are not given here.

2.3.6.1.4 Flux Path 4

The flux pattern in path 4 resembles that of the flux in path 2 except that it is advanced by $-\theta$ in all the computations of length and other variables; therefore, the derivations of flux path 2 can be referred to. The length of the flux lines and the cross section of their path in magnetic parts of the machine may be derived easily and are not given here. The length of the flux path in the back iron is given by the arc angle of $2\pi/3$ and not π. The magnetic equivalent circuit is identical to that of flux path 1 shown in Figure 2.25.

2.3.6.1.5 Flux Path 5

This is identical to flux path 1 in the stator pole. When it comes to the upper air gap between the stator and rotor poles, the length of the flux lines in the air gap increases; the length decreases in the lower stator and rotor pole pair. The length of the flux lines in the lower stator and rotor pole exactly corresponds to that of flux path 1 at the upper stator and rotor pole; therefore,

$$\ell_{g5\ell} = \ell_{g1u} \tag{2.194}$$

where ℓ_{g1u} has been derived in an earlier section and is given by Eq. (2.152). The cross section of the flux path is

$$A_{g5} = A_{g1} \tag{2.195}$$

As for the air gap length between the upper stator and rotor pole pair, it is identical to flux path 1 of the lower part stator and rotor pole pair, hence its length is given by:

$$\ell_{g5u} = \ell_{g1\ell} \tag{2.196}$$

The lengths of the flux path in the rotor pole and rotor back iron are identical to those of flux path 1. The equivalent circuit for this flux path is identical to the equivalent circuits of flux paths 1, 2, 3, and 4.

2.3.6.1.6 Flux Path 6

This flux path is dealt with in Section 2.3.2.7, and the equations and equivalent circuit from the same section are directly applicable here.

2.3.6.1.7 Inductance in Region 1

The inductance in region 1 is arrived at as:

$$L_a = \sum_{n=1}^{6} L_n \tag{2.197}$$

where $L_1, L_2, \ldots, L_6$ are the inductances contributed by the flux linkages associated with paths 1, 2,…,6, respectively.

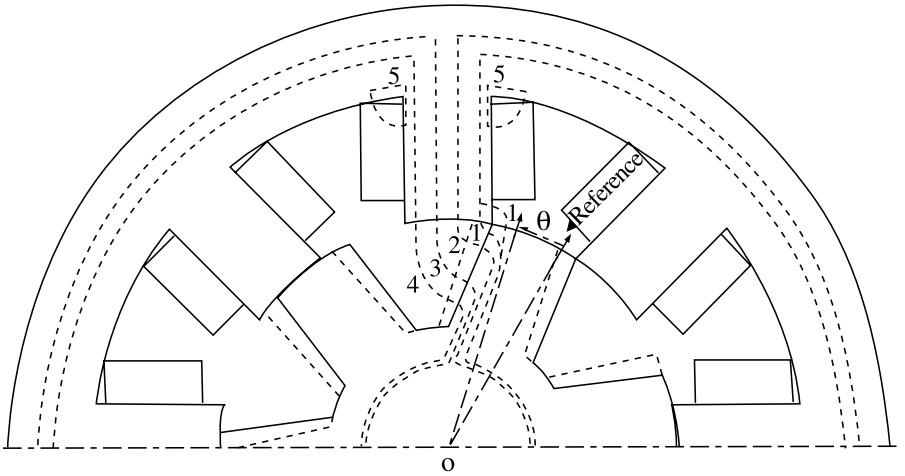

FIGURE 2.28 Flux distribution in region 2.

2.3.6.2 Region 2

Region 2 is defined by the rotor movement from its completely unaligned position, θ, as:

$$\frac{\theta_{rp} - (\beta_s + \beta_r)}{2} \le \theta \le \frac{\theta_{rp}}{2} \tag{2.198}$$

The typical flux distribution at an intermediate position in region 2 is shown in Figure 2.28. Only five flux paths are considered here. Many more can be included to improve the accuracy of predicting the machine characteristics. The chosen flux paths are explained in the following and their relevant lengths in the air gap are given.

2.3.6.2.1 Flux Path 1

This is similar to flux path 1 in region 1 in terms of its length and area of cross section in the stator and rotor poles. It is symmetric with respect to its diametrically opposite rotor pole and hence is not shown in the figure. Flux path 1 has two subpaths in the air gap with half of the flux lines in each subpath. The area of cross section of the flux path in the air is the average of the stator pole exit and rotor pole entrance cross sections and for subpath 1 is given by:

$$A_{g1} = \frac{1}{2}[A_{sp1} + A_{rp1}] = \frac{1}{2}\left[\frac{h_s}{4} + \frac{\beta_r}{4}\left(\frac{D}{2} - \ell_g\right)\right]L \tag{2.199}$$

For subpath 1′, the area of cross section is

$$\begin{aligned} A_{g1'} &= \frac{1}{2}\left[\frac{\beta_s}{4}\frac{D}{2} + \frac{h_r}{4}\right]L; \quad \left(\frac{\theta_{rp}}{2} - \frac{\beta_r}{2} - \frac{\beta_s}{2}\right) \le \theta \le \left(\frac{\theta_{rp}}{2} - \frac{\beta_r}{2} - \frac{3\beta_s}{8}\right) \\ &= \frac{\beta_s}{4}\frac{D}{2}L; \quad \left(\frac{\theta_{rp}}{2} - \frac{\beta_r}{2} - \frac{3\beta_s}{8}\right) \le \theta \le \frac{\theta_{rp}}{2} \end{aligned} \tag{2.200}$$

Note that the area of cross section of subpath 1′ is dependent on the rotor position and so also its reluctance. The lengths of the mean flux in these subpaths are derived assuming that the flux subpath entrance is at $\beta_r/4$ from the tip of the stator pole and are given as:

$$\ell_{g1u} = \ell_{g1\ell} = \frac{\pi}{3}\sqrt{(x_2 - x_1)^2 + (y_2 - y_1)^2}; \quad \left(\frac{\theta_{rp}}{2} - \frac{\beta_r + \beta_s}{2}\right) \le \theta \le \left(\frac{\theta_{rp}}{2} - \frac{\beta_s}{2} - \frac{1}{4}\beta_r\right)$$
$$= 0; \quad \left(\frac{\theta_{rp}}{2} - \frac{\beta_s}{2} - \frac{1}{4}\beta_r\right) \le \theta \le \frac{\theta_{rp}}{2} \tag{2.201}$$

$$\ell_{g1'u} = \ell_{g1'\ell} = \frac{\pi}{3}\sqrt{(x_4 - x_3)^2 + (y_4 - y_3)^2}; \quad \left(\frac{\theta_{rp}}{2} - \frac{\beta_r + \beta_s}{2}\right) \le \theta \le \left(\frac{\theta_{rp}}{2} - \frac{3\beta_s}{8} - \frac{\beta_r}{2}\right)$$
$$= \ell_g; \quad \left(\frac{\theta_{rp}}{2} - \frac{3\beta_s}{8} - \frac{\beta_r}{2}\right) \le \theta \le \frac{\theta_{rp}}{2} \tag{2.202}$$

where

$$x_1 = \frac{D}{2}\sin\left(\frac{\beta_s}{2}\right) \tag{2.203}$$

$$y_1 = \frac{h_r}{8} + \frac{D}{2}\cos\left(\frac{\beta_s}{2}\right) \tag{2.204}$$

$$x_2 = \left(\frac{D}{2} - \ell_g\right)\sin\left(\frac{\beta_s}{2} + \frac{\beta_r}{4}\right) \tag{2.205}$$

$$y_2 = \left(\frac{D}{2} - \ell_g\right)\cos\left(\frac{\beta_s}{2} + \frac{\beta_r}{4}\right) \tag{2.206}$$

$$x_3 = \frac{D}{2}\sin\left(\frac{3\beta_s}{8}\right) \tag{2.207}$$

$$y_3 = \frac{D}{2}\cos\left(\frac{3\beta_s}{8}\right) \tag{2.208}$$

$$x_4 = c_1 \sin\theta \tag{2.209}$$

$$y_4 = c_1 \cos\theta \tag{2.210}$$

$$c_1 = \frac{D}{2} - \ell_g - \frac{h_r}{8}\left\{1 - \frac{\theta}{\left(\frac{\theta_{rp}}{2} - \frac{\beta_r}{2} - \frac{3\beta_s}{8}\right)}\right\} \tag{2.211}$$

Therefore, the total length of the mean flux line in air is

$$\ell_{g1} = \ell_{g1u} + \ell_{g1\ell} = 2\ell_{g1u} \tag{2.212}$$

$$\ell_{g1'} = \ell_{g1'u} + \ell_{g1'\ell} = 2\ell_{g1'u} \tag{2.213}$$

The magnetic equivalent circuit is very similar to Figure 2.25 for subpaths 1 and 1′ and also for flux paths 2, 3, and 4. For brevity, it is omitted from now on.

2.3.6.2.2 Flux Path 2

The area of cross section for this flux path in the stator pole is

$$A_{sp2} = \frac{\beta_s}{4}\frac{D}{2}L \tag{2.214}$$

and in the rotor pole is

$$\begin{aligned} A_{rp2} &= \frac{h_r}{4}L; \quad \left(\frac{\theta_{rp}}{2} - \frac{(\beta_s + \beta_r)}{2}\right) \le \theta \le \left(\frac{\theta_{rp}}{2} - \frac{\beta_r}{2} - \frac{1}{8}\beta_s\right) \\ &= A_{sp2}; \quad \left(\frac{\theta_{rp}}{2} - \frac{\beta_r}{2} - \frac{1}{8}\beta_s\right) \le \theta \le \frac{\theta_{rp}}{2} \end{aligned} \tag{2.215}$$

The area of cross section of the flux path in the air gap is

$$A_{g2} = \frac{A_{sp2} + A_{rp2}}{2} \tag{2.216}$$

The length of the mean flux in air gap is

$$\ell_{g2u} = \ell_{g2\ell} = \sqrt{(x_6 - x_5)^2 + (y_6 - y_5)^2} \tag{2.217}$$

where

$$x_5 = \frac{D}{2}\sin\left(\frac{1}{8}\beta_s\right) \tag{2.218}$$

$$y_5 = \frac{D}{2}\cos\left(\frac{1}{8}\beta_s\right) \tag{2.219}$$

$$x_6 = c_2 \sin\theta \tag{2.220}$$

$$y_6 = c_2 \cos\theta \tag{2.221}$$

$$c_2 = \frac{D}{2} - \ell_g - \frac{3}{8}h_r\left(1 - \frac{\theta}{\frac{\theta_{rp}}{2} - \frac{\beta_r}{2} - \frac{1}{8}\beta_s}\right); \quad \left(\frac{\theta_{rp}}{2} - \frac{\beta_r}{2} - \frac{\beta_s}{2}\right) \le \theta \le \left(\frac{\theta_{rp}}{2} - \frac{\beta_r}{2} - \frac{1}{8}\beta_s\right) \tag{2.222}$$

$$\ell_{g2u} = \ell_g; \quad \left(\frac{\theta_{rp}}{2} - \frac{\beta_r}{2} - \frac{1}{8}\beta_s\right) \le \theta \le \frac{\theta_{rp}}{2} \tag{2.223}$$

The total air gap length for both the upper and lower rotor and stator poles for this path is

$$\ell_{g2} = \ell_{g2u} + \ell_{g2\ell} = 2\ell_{g2u} \tag{2.224}$$

2.3.6.2.3 Flux Path 3

This path has a width of $(\beta_s/4)(D/2)$ in the stator pole, as the flux paths 2 and 3, and has the same width at the rotor entrance when the rotor interpolar space is closer than a side of the rotor pole. If the side of the rotor pole is nearer, the width of its entry is $(h_r/4)$. The area of cross section of the flux path in air is

$$A_{g3} = \frac{1}{2}[A_{sp3} + A_{rp3}] \tag{2.225}$$

where

$$A_{sp3} = \frac{\beta_s}{4}\frac{D}{2} \cdot L \tag{2.226}$$

$$\begin{aligned} A_{rp3} &= \frac{h_r}{4}L; \quad \text{if flux path is through rotor side} \\ &= A_{sp3}; \quad \text{if flux path is through rotor interpolar} \\ &\qquad \text{space or directly through rotor pole face} \end{aligned} \tag{2.227}$$

Whether the flux path is through the rotor side or rotor interpolar (between two rotor poles) space is determined by the following algorithm for the air gap length:

$$\ell_{g3u} = \ell_{g3\ell} = \frac{\ell_{g3}}{2} \tag{2.228}$$

where

$$\frac{\ell_{g3}}{2} = \frac{\pi}{3}\sqrt{(x_8 - x_7)^2 + (y_8 - y_7)^2}; \quad \text{if } \frac{\ell_{g3}}{2} \le \left(\frac{D}{2} - \ell_g - h_r\right) \tag{2.229}$$

otherwise,

$$\frac{\ell_{g3}}{2} = \left(\frac{D}{2} - \ell_g - h_r\right) \tag{2.230}$$

and

$$x_7 = \frac{D}{2}\sin\left(\frac{-\beta_s}{8}\right) \tag{2.231}$$

$$y_7 = \frac{D}{2}\cos\left(\frac{-\beta_s}{8}\right) \tag{2.232}$$

$$x_8 = c_3 \sin\left(\frac{\theta_{rp}}{2} - \frac{\beta_r}{2} - \theta\right) \tag{2.233}$$

$$y_8 = c_3 \cos\left(\frac{\theta_{rp}}{2} - \frac{\beta_r}{2} - \theta\right) \tag{2.234}$$

$$c_3 = \frac{D}{2} - \ell_g - \frac{5}{8}h_r\left(1 - \frac{\theta}{\frac{\theta_{rp}}{2} - \frac{\beta_r}{2} + \frac{1}{8}\beta_s}\right); \quad \left(\frac{\theta_{rp}}{2} - \frac{\beta_s + \beta_r}{2}\right) \le \theta \le \left(\frac{\theta_{rp}}{2} - \frac{\beta_r}{2} + \frac{1}{8}\beta_s\right) \tag{2.235}$$

Flux path 3 presents three air gap choices when (1) it enters interpolar space, (2) it enters the side of the rotor pole, and (3) it enters on the rotor pole face. Both case (1) and (2) have been addressed in Eqs. (2.229) and (2.230). When the leading rotor pole barely reaches the exit of the mean flux path in the stator pole, note that the air gap is reduced to the air gap during alignment, giving rise to case (3), hence the air gap at that time is

$$\frac{\ell_{g3}}{2} = \ell_g; \quad \left(\frac{\theta_{rp}}{2} - \frac{\beta_r}{2} + \frac{1}{8}\beta_s\right) \le \theta \le \frac{\theta_{rp}}{2} \tag{2.236}$$

This is the third case for the air gap length of flux path 3.

2.3.6.2.4 Flux Path 4

This flux path has characteristics very similar to flux path 3, with the same three possibilities for its air gap. Derivations for its air gap length and area of cross section are omitted for the sake of brevity.

2.3.6.2.5 Flux Path 5

This flux path is identical to flux path 7 in the case of unaligned inductance evaluation; therefore, it is not further reviewed here.

2.3.6.2.6 Inductance Evaluation

The procedure for inductance and flux linkages determination is very similar to that for the unaligned and aligned cases covered earlier in this chapter. No further consideration is given here for application to regions 1 and 2 to avoid repetition.

2.4 SECONDARY FLUX PATHS

Hitherto, the inductance evaluation has been based only on two-dimensional flux distribution. The various flux paths at both ends of the stator and rotor poles and the varieties of ways they can traverse have been ignored. In terms of their influence, the studies have indicated their contribution to inductances can amount to as much as 15% of unaligned inductance. Their significance near aligned positions is relatively very small compared to the inductance value at these positions, even though their absolute magnitude may remain constant. Small errors can arise due to the omission of such fringing and end effects in performance evaluations, and the error introduced may be on the order of 3 to 5% of the peak rating of the machine. Studies have yet to emerge to predict very precisely the effects of secondary flux path omissions on the computation of machine performance. To alleviate this circumstance, we resort to three-dimensional finite element analysis. It provides very little insight to a designer seeking the cause–effect relationships among a set of machine dimensions, excitation and rotor positions, and the resulting set of machine characteristics and performance.

An analytical method similar to the approach developed using magnetic equivalent circuits allows inclusion of the inductance contribution of the secondary flux paths. A number of such predetermined paths have been developed in earlier texts,[13] and Appendix 3A contains some flux path and permeance computational formula that can be used to enhance the accuracy of prediction. In Chapter 3, they are used for inductance prediction of linear switched reluctance machines. The equations and approach are easier to use for linear machines than for rotary machines (see Chapter 3).

2.5 COMPUTATION OF INDUCTANCE

The algorithms derived for inductance prediction in this chapter have to be carefully coded. The transitions between regions 1 and 2 and the varying length of flux paths in the stator, rotor and air gap require special attention, as they involve various cases for different rotor positions. The algorithms for regions 1 and 2 indicate, in general, a simple procedure for the derivation of equations for inductance prediction. They should

be used more as a guideline rather than for direct use in the design process. For higher accuracy in prediction, a larger number of flux paths is necessary and are therefore strongly recommended for those interested in mechanizing this procedure for their day-to-day SRM design use.

The accuracy of prediction of the three-dimensional characteristics of the flux linkages vs. excitation current vs. rotor position is within 5 to 10% of the measured results. The accuracy can be improved with selecting a higher number of flux paths. The only advantage of this method of finding machine characteristics is in assessing new machine configurations and their impact on the machine characteristics. For example, the machine characteristics can be changed by modifying only a segment of the stator or rotor or both of them in the machine and changing its flux path. In such a circumstance, the direct relationship between the machine dimensional changes and the machine characteristic changes can be captured using the method developed in this chapter, leading to a qualitative and quantitative understanding of the machine and its design.

REFERENCES

1. Miller, T.J.E. and M. McGilp, Nonlinear theory of the switched reluctance motor for rapid computer-aided design, *IEE Proc. B,* 137(6), 337–346, 1990.
2. Lindsay, J.F., R. Arumugam, and R. Krishnan, Finite element analysis characterization of a switched reluctance motor with multi-tooth per stator pole, *IEE Proc. B,* 133(6), 347–353, 1986.
3. Corda, J. and J.M. Stephenson, An analytical estimation of the minimum and maximum inductances of a double-salient motor, in *Proc. of the Int. Conf. on Stepping Motors and Systems,* Leeds, 1979, pp. 50–59.
4. Radun, A., Analytical calculation of the switched reluctance motor's unaligned inductance, *IEEE Trans. on Magnetics,* 35(6), 4473–4481, 1999.
5. Stephenson, J.M. and J. Corda, Computation of torque and current in doubly salient reluctance motors from nonlinear magnetization data, *IEEE Proc.,* 127(5), 393–396, 1979.
6. Esatham, A.R., H. Yuan, G.E. Dawson, P.C. Choudhury, and P.M. Cusack, A finite element evaluation of pole shaping in switched reluctance motors, *Electrosoft,* 1(1), 55–67, 1990.
7. Arumugam, R., D.A. Lowther, R. Krishnan, and J.F. Lindsay, Magnetic field ananlysis of a switched reluctance motor using a two-dimensional finite element model, *IEEE Trans. on Magnetics,* Vol. MAG-21, No. 5, 1883–1885, 1985.
8. Arumugam, R., Design and Finite Element Analysis of Switched Reluctance Motors, Ph.D. thesis, Concordia University, Montreal, Canada, December 1987.
9. Lee, B.-S., H.-K. Bae, P. Vijayraghavan, and R. Krishnan, Design of a linear switched reluctance machine, in *IEEE Ind. Appl. Soc. Conf.* (*IAS '99*), Vol. 4, Oct. 3–7, 1999, Phoenix, AZ, pp. 2267–2274.
10. Krishnan, R., M. Abou-Zeid, and X. Mang, A design procedure for axial field switched reluctance motors, in *IEEE Ind. Appl. Soc. Ann. Mtg. Conf. Rec.,* Oct. 1990, Seattle, WA, pp. 241–246.
11. Materu, P. and R. Krishnan, Analytical prediction of SRM inductance profile and steady state average torque, in *IEEE Ind. Appl. Soc. Ann. Mtg. Conf. Rec.,* Oct. 1990, Seattle, WA, pp. 214–223.

12. Deshpande, U.S., J.J. Cathey, and E. Richter, A high force density linear switched reluctance machine, in *Conf. Rec. of the 1993 IEEE IAS Ann. Mtg.,* Vol. 1, Oct. 1993, Toronto, Canada, pp. 251–257.
13. Roters, H.C., *Electromagnetic Devices,* Wiley, New York, 1941.
14. Corda, J. and M. Wilkinson, Prediction and measurement of magnetic parameters of cylindrical linear switched reluctance actuator, in *Proc. of Int. Conf. on Electrical Machines,* Vol. 3, Sept. 1994, Paris, France, pp. 479–484.
15. Lee, B.S., Linear Switched Reluctance Machine Drives with Electromagnetic Levitation and Guidance Systems, Ph.D. thesis, The Bradley Department of Electrical and Computer Engineering, Virginia Tech., Blacksburg, VA, Nov. 2000.